Journal of Medicinal Chemistry

Article

Discovery of Novel Pyrazolo[3,4-b] pyridine Derivatives with Dual Activities of Vascular Remodeling Inhibition and Vasodilation for the Treatment of Pulmonary Arterial Hypertension

Liqing Hu, Lijun Li, Qi Chang, Songsen Fu, Jia Qin, Zhuo Chen, Xiaohui Li, Qinglian Liu, Gaoyun Hu, and Qianbin Li

J. Med. Chem., **Just Accepted Manuscript** • DOI: 10.1021/acs.jmedchem.0c01132 • Publication Date (Web): 11 Sep 2020

Discovery of Novel Pyrazolo[3,4-*b*] pyridine Derivatives with Dual Activities of Vascular Remodeling Inhibition and Vasodilation for the Treatment of Pulmonary Arterial Hypertension

Liqing Hu,[1,3] Lijun Li,[2] Qi Chang,[1] Songsen Fu,[1] Jia Qin,[1] Zhuo Chen,[1] Xiaohui Li,[2] Qinglian liu,[3] Gaoyun Hu,[1] and Qianbin Li*,[1]

[1] Department of Medicinal Chemistry, Xiangya School of Pharmaceutical Sciences, Central South University, Changsha 410013, Hunan, China

[2] Department of Pharmacology, Xiangya School of Pharmaceutical Sciences, Central South University, Changsha 410013, Hunan, China

[3] Department of Physiology and Biophysics, School of Medicine, Virginia Commonwealth University, VA 23298, USA

ABSTRACT

Current pulmonary arterial hypertension (PAH) therapeutic strategies mainly focus on vascular relaxation with less emphasis on vascular remodeling, which results in poor prognosis. Hence, dual pathway regulators with vasodilation effect via soluble guanylate cyclase (sGC) stimulation and vascular remodeling regulation effect by AMP-activated protein kinase (AMPK) inhibition will provide more advantages and potentialities. Herein, we designed and synthesized a series of novel pyrazolo[3,4-*b*] pyridine derivatives based on sGC stimulator and AMPK inhibitor scaffolds. *In vitro*, **2** exhibited moderate vasodilation activity and higher proliferation and migration suppressive effects compared to riociguat. *In vivo*, **2** significantly decreased right ventricular systolic pressure

(RVSP), attenuated pulmonary artery medial thickness (PAMT) and right ventricular hypertrophy (RVH) in hypoxia-induced PAH rat models (i.g.). Given the unique advantages of significant vascular remodeling inhibition and moderate vascular relaxation based on dual pathways regulation, we proposed **2** as a promising lead for anti-PAH drug discovery.

INTRODUCTION

Pulmonary arterial hypertension (PAH) is a type of chronic progressive and life-threatening cardiopulmonary disease with annual mortality about 15% in high-risk patients.[1, 2] PAH is characterized by pulmonary vascular remodeling, elevated pulmonary vascular resistance (PVR) and increased pulmonary artery pressure (PAP), resulting in right ventricular overload and hypertrophy, and eventually right heart failure or even death.[3, 4]

It is widely recognized that advances in PAH pathology contributed enormously to the identification of several effective therapeutic targets, including endothelin pathway, prostacyclin pathway, and nitric oxide (NO) pathway.[5-9] However, despite considerable progress in conventional therapies or newly developed targeted therapies, these treatment strategies mainly focus on vasodilation to reduce blood pressure. As a result, the side effects on systemic hypotension and bottlenecks in efficiency remain challenging clinical problems, which still lead to poor prognosis.[10] The main reason lies in the lack of efficient treatment strategies targeting pulmonary vascular remodeling. With the increasing understanding on the pathological biology of PAH, vascular remodeling has been recognized as the essential pathological characteristic of PAH over the past decade.[11, 12] It is noteworthy that the excessive proliferation and abnormal migration of human pulmonary arterial smooth muscle cells (HPASMCs) and human lung fibroblasts (HLF1) are pivotal abnormal

phenotypes of PAH. These abnormalities will thicken the pulmonary vascular wall and ultimately result in occlusion and fibrosis of vascular.[13, 14]

In terms of PAH clinical manifestations, high PAP is the primary factor to be dealt with. The heart overload can be reduced with decreased ventricular pressure, which also results in the improvement of blood flow and alleviation of hypoxia status. Soluble guanylate cyclase (sGC), the endogenous receptor of NO, is attracting tremendous enthusiasm in PAH drug discovery. sGC stimulation not only promotes vasodilation but also slightly inhibits vascular remodeling via increasing the level of messenger molecule cGMP.[15, 16] These pharmacological effects make sGC/cGMP a typical signaling pathway in the treatment of PAH through regulating a number of downstream targets such as protein kinases, cyclic nucleotide-gated channels and phosphodiesterases.[8, 17] sGC stimulators, a class of ligands that bind allosterically to the heme-containing sGC, act NO-independently to stimulate the formation of cGMP.[15] Riociguat (Adempas®) (Figure 1), the first approved sGC stimulator for treating PAH, significantly decreased mean pulmonary artery pressure (mPAP) and PVR, and improved right ventricular function.[18,19] Although riociguat displays many advantages in attenuating the symptoms of PAH, it is insufficient to block PAH progression due to its limited inhibition of vascular remodeling. Moreover, the systematic hypotension partially due to high level of cGMP suggests its limited clinical use. [20, 21]

To overcome the drawbacks of monotherapy by vasodilation, the strategy majorly targeting vascular remodeling will be a potential addition. In fact, many attempts and efforts to treat PAH by means of inhibiting vascular remodeling have been investigated. Adenosine monophosphate-activated protein kinase (AMPK) is a serine-threonine kinase, well known as cellular energy homeostasis regulator.[22] Previous reports have shown that AMPK activation and activity is induced early and

remains elevated in cancer cells, which is essential for cell growth and proliferation. However, AMPK is not required for growth in normal cells with abundance of nutrients.[23] Genetic deletion of AMPK or attenuation of its activity in tumor cells was sufficient to reduce cell proliferation. Interestingly, the increased AMPK activation was determined by AMPK phosphorylation at the residue Thr172, required for the mammalian AMPK activation, and the higher AMPK activity was assessed by acetyl-CoA carboxylase (ACC) phosphorylation at the residue Ser79.[23] Particularly, AMPK plays a key role in abnormal cell phenotypes of HPASMCs and HLF1 under conditions such as hypoxia or drug induction.[24, 25] The level and activity of phosphorylated AMPK (p-AMPK) in HPASMCs of PAH and hypoxic mouse PASMCs appeared to be elevated. The over-activated AMPK promotes cell metabolism by increasing ATP consumption, leading to abnormal cell proliferation and migration, and ultimately vascular remodeling.[26] Moreover, compound C (Figure 1), an AMPK inhibitor, prevents hypoxia-induced PAH *in vivo*.[24] These results suggest that AMPK pathway may be a significant therapeutic target in the treatment of PAH through inhibiting vascular remodeling.[24, 26]

In recent years, it has been reported that monotherapy via vascular remodeling inhibition results in rapid changes of vascular status. This in turn promotes a vicious circle, leading to the failure of PAH treatment.[27-29] Combination therapy has been widely accepted as simultaneous regulation of vascular remodeling and vasodilation to produce improved outcomes compared to monotherapy.[30] Interestingly, the novel hybrid (CDDO-NO, Figure 1) from bardoxolone methyl (CDDO-Me) and NO donor exhibited dual actions of vascular remodeling inhibition and pulmonary vascular relaxation, which was superior to the mono- or combination therapy.[31]

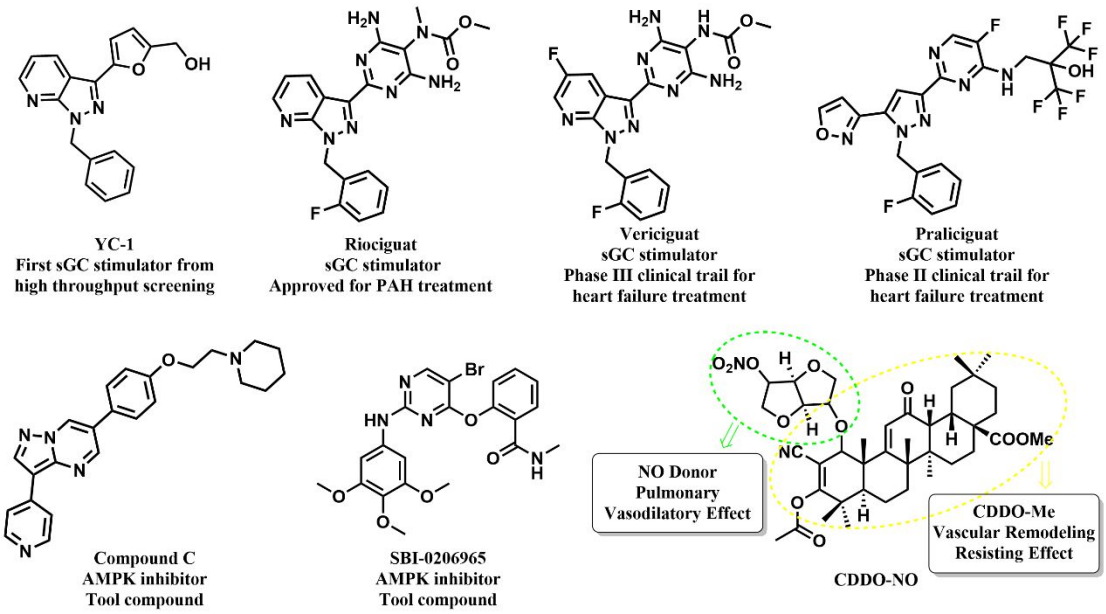

Figure 1. Structures of sGC stimulators, AMPK inhibitors and CDDO-NO.

To find novel dual regulators of both high ventricular pressure and vascular remodeling, sGC and AMPK pathways will be the focus in this study. In modern drug discovery, fragment-based drug design (FBDD) strategy provides many opportunities for the rational development of drug candidates. Previously, it was reported that pyrazolo[3,4-*b*]pyridine derivatives have strong anti-proliferation effect.[32] Furthermore, as shown in Figure 1, the pyrimidine and benzyl moieties were vital for potent sGC stimulation based on extensive structure-activity relationship (SAR) studies.[10, 33] In addition, the pyrazolo[1,5-*a*]pyrimidine scaffold in the structure of compound C has been suggested to bound tightly to a unique elongated binding pocket of AMPK enzyme, while the piperidine ring resides outside the binding pocket.[34] These integrated information led to the discovery of the lead compound 5-(4,6-diaminopyrimidin-2-yl)-3-methyl-1-phenyl-1,7-dihydro-6*H*-pyrazolo[3,4-*b*] pyridin-6-one (**1**, Figure 2). Consistent with our hypothesis, compound **1** exhibited considerable inhibition against both the HPASMCs and HLF1 proliferation compared to riociguat and compound C.

Herein, we purposely optimized the structure of **1** to improve its potency using fragment linking and growing strategies (Figure 2). The subsequent screening based on pre-constricted rat thoracic aorta rings and cell viability assays resulted in the discovery of **2** with moderate vasodilatory effect compared with riociguat and significant improved inhibitory activity against HPASMCs and HLF1 proliferation and migration compared to compound C. Compound **2** demonstrated moderate regulatory effect on sGC/cGMP pathway and considerable inhibition against AMPK signaling pathway, which resulted in equivalent RVSP control, better RVH and PAMT improvement *in vivo*.

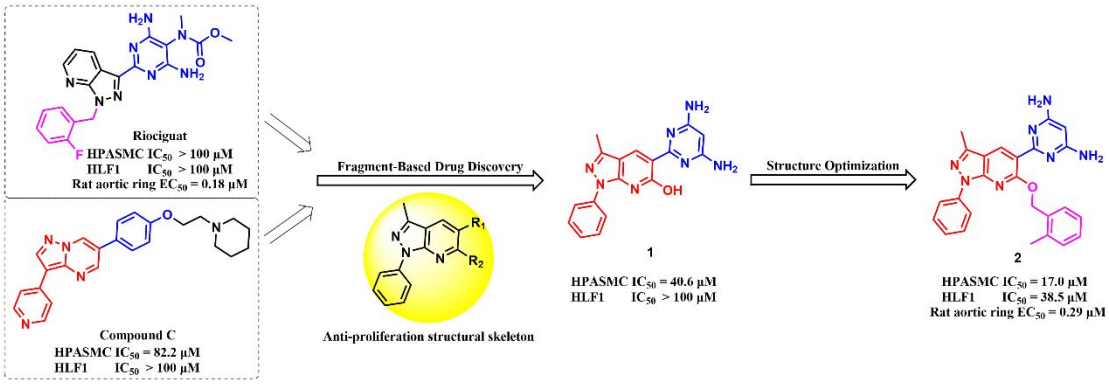

Figure 2. Design rationale and optimization of pyrazolo[3,4-*b*] pyridine derivatives with dual activities of anti-vascular remodeling and regulating vascular tone.

CHEMISTRY

All targeted compounds were prepared with high yields following synthetic routes outlined in Schemes 1-5. The key intermediates **10**, **14a-i** (Scheme 1), and **16**, **20a-d** (Scheme 2) were synthesized with initial efforts. As shown in Scheme 1, compound **4** was synthesized through Vilsmeier-Haack-Arnold reaction with **3** as the starting material, and the chlorine was substituted by azide to afford **5**, followed by the reduction of **5** to acquire the intermediate **6**. **7** was the substitution reaction product through introducing benzyl group on **6** and the subsequent *N*-alkylation

product **8** can be obtained via reacting **7** with ethyl cyanoacetate. 3-methyl-6-oxo-1-phenyl-6,7-dihydro-1*H*-pyrazolo[3,4-*b*]pyridine-5-carbonitrile (**11**) was provided by the reaction of compound **6** and ethyl cyanoacetate in acetic acid.[35] Actually, we did not directly obtain *N*-alkylation product **8** from compound **11**, but only *O*-alkylation product **12a-i** even through different bases such as potassium carbonate, cesium carbonate and sodium hydride. We speculated that the presence of phenyl group on N1 of **11** might increase the steric hindrance, resulting in the only formation of *O*-alkylation products. Reducing cyano-group is a crucial step to introduce pyrimidine ring. Compounds **9** or **13a-i** were the reaction products of hydroxylamine hydrochloride and **8** or **12a-i**. The key intermediates **10** and **14a-i** were from **9** and **13a-i**, respectively.[36, 37] The synthetic approach for substituted-malononitrile compounds **16** and **20a-d** is outlined in Scheme 2 by referring to relevant literatures.[38, 39]

Scheme 1. Synthesis of 3-methyl-1-phenyl-1*H*-pyrazolo[3,4-b] pyridine-5-carboximidamides 10 and 14a-i[a]

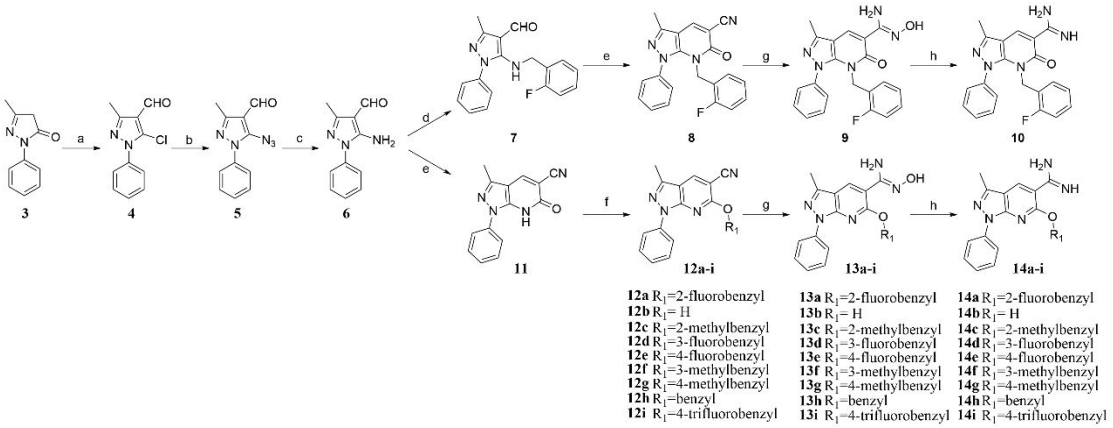

[a]Reagents and conditions: (a) DMF, $POCl_3$, 100 ℃, 2 h; (b) NaN_3, TBAI, DMSO, rt, 18 h; (c) Fe (power), NH_4Cl, EtOAc, H_2O, rt, 22 h; (d) CH_3CN, K_2CO_3, rt, 4 h; (e) $NCCH_2COOEt$, AcOH, reflux, 48 h; (f) DMF, K_2CO_3, rt, 2 h; (g) H_2NOH-HCl, DIEA, EtOH, 90 ℃, Ar, 24 h; (h) Zn, AcOH, rt, 8 h.

Scheme 2. Synthesis of substituted-malononitrile intermediates 16 and 20a-d[a]

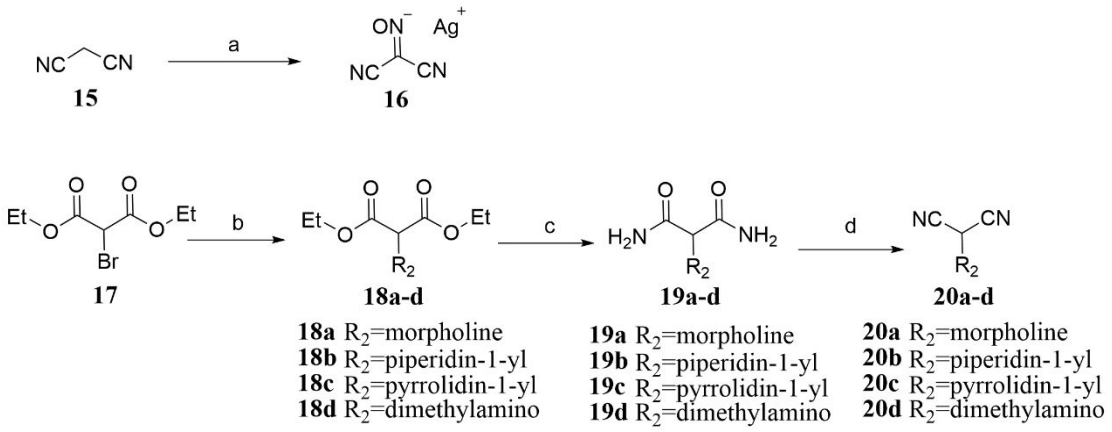

[a]Reagents and conditions: (a) $NaNO_2$, AcOH, H_2O, $AgNO_3$, rt, 12 h; (b) K_2CO_3, CH_3CN, rt, 3 h; (c) NH_3, MeOH, rt, 48 h; (d) $POCl_3$, DMF, -5 ~ 0 ℃, 4 h.

As a proof of concept, a series of targeted compounds were designed and synthesized by introducing the 4,6-diamino-pyrimidine rings so as to increase sGC stimulating activity. The crucial step for each route was the synthesis of substituted-pyrimidines, such as **21a-e**, **25a-d** (Scheme 3), or **1**, **2**, **31a-f** (Scheme 5). After brief investigation, synthetic methodology for preparing this pyrimidine scaffold has been validated.[40] The reaction of **10** or **14a-i** with **15** that was commercially available or the appropriate malononitrile derivatives **20a-d**, which were prepared according to Scheme 2, under microwave irradiation at 130 °C to afford 4,6-diamino-pyrimidines **1**, **2**, **21a-e**, **30** and **31a-f**. In addition, compound **23** was the product of the cyclization of **22** and **16** followed by the removal of silver chloride using a pyrimidine forming procedure,[41] and subsequent reduction of the resulting nitroso group with Zn powder furnished the target **24** (Scheme 3). Treatment of the resulting tri-aminopyrimidine with acyl chloride compounds delivered products **25a-d** and **27** (Scheme 4). Target compound **29** was prepared under the reaction of **25b** with iodomethane catalyzed by sodium hydride (Scheme 4).

Scheme 3. Synthesis of 2-(6-((2-fluorobenzyl)oxy)-3-methyl-1-phenyl-1*H*-pyrazolo[3,4-*b*]pyridin-5-yl)pyrimidine-4,6-diamine derivatives 21a-e, 24 and 25a-d[a]

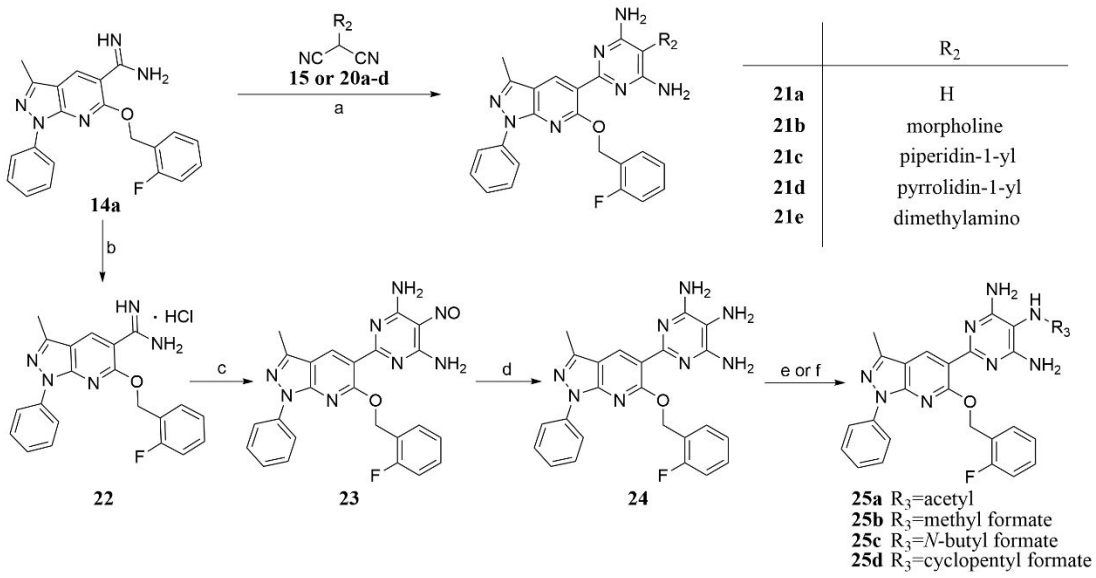

[a]Reagents and conditions: (a) Microwave (MW), MeOH, 1,4-dioxane, 130 ℃, 2 h; (b) HCl(gas), MeOH, rt, 2 h; (c) **16**, MeOH, rt, 2 h, 2-Methylpyridine, reflux, 30 min; (d) Zn, EtOAc, AcOH, rt, 8 h; (e) K_2CO_3, CH_3CN, -5 ~ 0 ℃, 1 h to rt 2 h (**25a**); (f) Pyridine, -5 ~ 0 ℃, 2 h (**25b-d**).

Scheme 4. Synthesis of Compounds 27, 29 and 30[a]

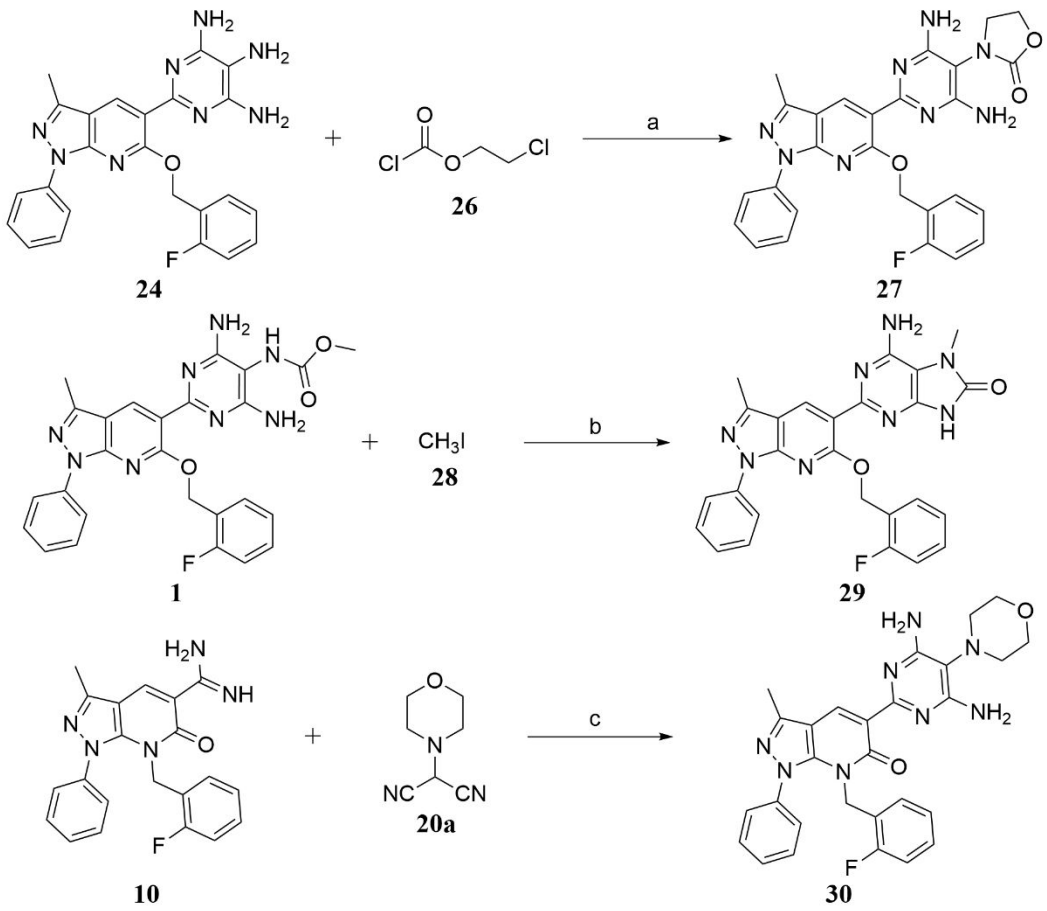

[a]Reagents and conditions: (a) K_2CO_3, CH_3CN, -5 ~ 0 ℃, 1 h to rt 2 h; (b) NaH, DMF, -5 ~ 0 ℃, 2 h; (c) Microwave (MW), MeOH, 1,4-dioxane, 130 ℃, 2 h.

Scheme 5. Synthesis of Compounds 1, 2 and 31a-f[a]

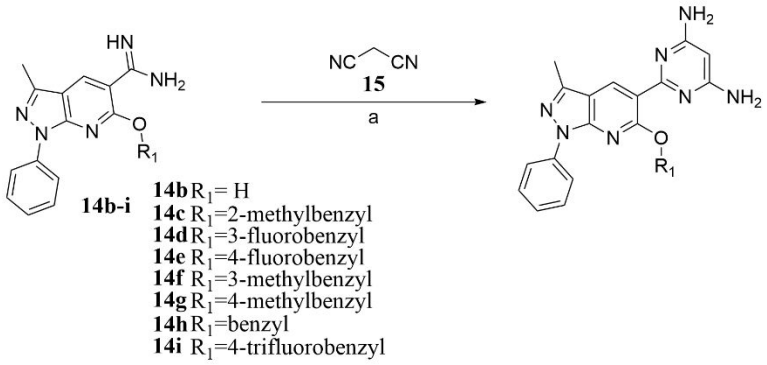

	R_1
1	H
2	2-methylbenzyl
31a	3-fluorobenzyl
31b	4-fluorobenzyl
31c	3-methylbenzyl
31d	4-methylbenzyl
31e	benzyl
31f	4-trifluorobenzyl

[a]Reagents and conditions: (a) Microwave (MW), MeOH, 1,4-dioxane, 130 ℃, 2 h.

RESULTS AND DISCUSSION

Rational Design of Novel Pyrazolo[3,4-*b*] pyridines to Improve Anti-proliferation Efficacy and

Vasodilatory Effect by Introducing Pyrimidine Pharmacophore. Increasing studies in recent years have demonstrated that the abnormal proliferation and migration of HPASMCs and HLF1 are the essential features of pulmonary vascular remodeling in the pathogenesis of PAH.[16, 42, 43] Considering these basic findings,[10, 32] we hypothesized that the introduction of pyrimidine groups on the basis of pyrazolo[3,4-*b*]pyridine ring could dramatically increase the effect of stimulating sGC, which mainly mediates vascular tone. Meanwhile, the designed compounds may also concomitantly inhibit AMPK to increase the effect of anti-vascular remodeling, which is crucial for better PAH treatment described above. Therefore, the priority of this study was to investigate the anti-proliferation effects of compounds against HPASMCs and HLF1 through the cell-based activity. Riociguat and compound C were applied as the positive control. As our initial effort, we prepared a novel pyrazolo[3,4-*b*] pyridine compound (**1**, IC_{50} = 40.6 μM), which had a marked improvement against HPASMCs proliferation compared with compounds **11** (IC_{50} > 100 μM) and **12a** (IC_{50} >100 μM). It is clear that introduction of pyrimidine ring replacing the cyano group at the 3-position of the pyridine ring significantly decreased the cell viability of HPASMCs, indicating that the pyrimidine moiety of **1** is essential for anti-proliferation activity (Table 1). In view of the considerable anti-proliferation effects of **1** against both HPASMCs and HLF1 compared to compound C, further structural modification was carried out in order to improve the anti-proliferation activity. Subsequently, compounds with better anti-proliferation activity were subjected to evaluating their ability to relax blood vessels based on the consideration of searching for compounds with moderate vasodilatory effect compared to riociguat.

Table 1. In Vitro SARs of Pyrazolo[3,4-*b*]pyridines Substituent Groups.

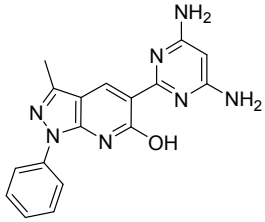

1

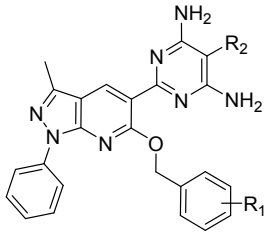

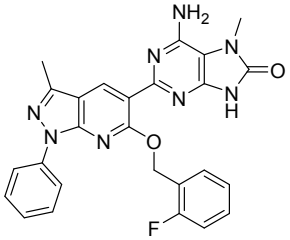

29

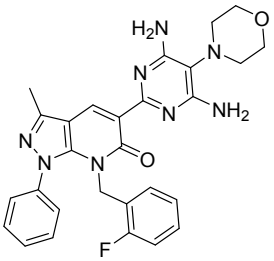

30

Compd.	R_1	R_2	HLF1 IC_{50} (μM)	HPASMC IC_{50} (μM)	Rat aortic ring EC_{50} (μM)	Emax (1μM, %)
1	--	--	>100	40.6±4.1	nd	nd
21a	2-F	H	55.6±1.3	59.3±5.3	2.2±0.1	41.3±2.9
21b	2-F		>100	25.2±1.6	8.2±0.2	28.7±7.4
21c	2-F		>100	53.0±3.0	0.79±0.02	47.8±5.5
21d	2-F		>100	29.3±0.8	12.7±1.1	29.8±7.7
21e	2-F		>100	56.5±5.5	1.1±0.1	46.1±7.3
24	2-F	$-NH_2$	37.2±0.8	22.4±1.3	0.96±0.02	46.7±9.9
25a	2-F		>100	34.9±1.8	0.93±0.01	51.1±10.1
25b	2-F		>100	25.5±1.2	5.8±0.2	31.4±13.7
25c	2-F		52.8±2.0	21.7±0.9	>100	15.8±4.1
25d	2-F	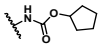	63.4±3.1	24.8±2.0	>100	15.5±9.4
27	2-F		49.7±0.5	24.7±1.3	>100	19.7±7.2
29	--	--	>100	23.2±1.2	4.9±0.2	32.9±10.4
30	--	--	>100	>100	nd	nd
31a	3-F	H	67.7±9.8	68.4±3.0	0.36±0.02	59.9±13.4
31b	4- F	H	55.3±2.0	>100	nd	nd

31c	3-Me	H	41.9±3.5	32.0 ±1.6	0.99±0.01	48.4±10.0
31d	4-Me	H	>100	89.4±6.5	nd	nd
31e	H	H	52.8±1.9	67.4±5.0	10.8±1.2	20.4±5.2
31f	4-CF_3	H	31.0±2.6	20.4±1.2	1.6±0.2	43.4±11.6
2	2-Me	H	38.5±0.2	17.0±1.0	0.29±0.05	63.2±3.7
C	--	--	>100	82.2±0.5	nd	nd
Riociguat	--	--	>100	>100	0.18±0.05	93.6±3.9

nd: not determined

In Vitro Structure-Activity Relationships (SARs) of Novel Pyrazolo[3,4-*b*]pyridine Derivatives. In view of the fundamental roles of HPASMCs and HLF1 abnormal proliferation in the pathogenesis of PAH, SAR studies were started to explore their inhibitory activities on cell viability using CCK-8 assay. Moreover, the aim of SAR studies was to find compounds with good inhibitory activities against both HPASMCs and HLF1 cell lines. The preliminary results indicated that the activity of *O*-alkylation product (**21b**, IC_{50} = 25.2 μM) is stronger than *N*-alkylation target (**30**, IC_{50} >100 μM) against HPASMCs. Hence, we focused on designing and synthesizing *O*-alkylation target compounds in a follow-up study. As shown in Table 1, most of the target compounds exhibited potent anti-proliferation activities, which were more effective than compound C and riociguat.

The initial investigation on the SARs of the pyrazolo[3,4-*b*]pyridine derivatives was mainly carried out by substituting the 5-position of the pyrimidine ring, and the inhibition activities of these substituted compounds against vascular hyper-proliferation cell lines were also presented in Table

1. Compounds with different substituents at the 5-position of the pyrimidine ring displayed a stronger inhibitory effect on HPASMCs proliferation than HLF1 which also abnormally proliferate in the pathogenesis of PAH. Compounds **21a** (**HFL1**, IC_{50} = 55.6 μM) and **24** (**HFL1**, IC_{50} = 37.2 μM) with a hydrogen and an amino group at the 5-position of the pyrimidine ring, respectively, showed potent anti-proliferation activities, while compounds **21b-e** (IC_{50} > 100 μM) bearing an aliphatic amine groups decreased significantly in potency toward HLF1, suggesting that a steric hindrance substitution at this position is unfavorable. Based on these results, further SARs were carried out through changing substituted groups at the benzyl in order to preferentially increase the inhibitory effect on HLF1, and the results are summarized in Table 1. The classic bioisosterism replacement of fluorine (**21a**, **HFL1**, IC_{50} = 55.6 μM; **HPASMC**, IC_{50} = 59.3 μM) with the methyl group (**2**, **HFL1**, IC_{50} = 38.5 μM; **HPASMC**, IC_{50} = 17.0 μM) resulted in an increased potency. Substitutions of the benzyl ring with fluorine atom or methyl group showed a preference at 2-position over other positions for the anti-proliferation activities, compounds **21a** and **2** versus compounds **31a-b** and **31c-d**, respectively. The electron withdrawing groups were beneficial to anti-proliferation activities against HLF1(**31f**, **-CF_3**, IC_{50} = 31.0 μM > **31b**, **-F**, IC_{50} = 55.3 μM > **31d**, **-CH_3**, IC_{50} > 100 μM). Taken together, compounds **24**, **31f** and **2** showed comparable anti-proliferation activities against both HPASMCs and HLF1.

Furthermore, we carried out the rat aortic ring assay to evaluate the vasodilation activity of the potential compounds. As shown in Table 1, the vasodilatory effect of compounds in different concentrations were measured and the EC_{50} was calculated. Results showed that the anti-proliferation activities of the compounds were not in agreement with the vasodilatory activity. We speculated that the newly designed and synthesized compounds have different effects based on the

dual target actions. Comparing with riociguat (IC_{50} > 100 μM), **25b** exhibited more potent anti-proliferation activity against HPASMCs (IC_{50} = 25.5 μM), with a weak vasodilatory effect (**25b**, EC_{50} = 5.8 μM; **riociguat**, EC_{50} = 0.18 μM). These results provide an experimental basis for us to search for further compounds with better anti-proliferation activities and moderate vasodilatory effect compared to riociguat. The anti-proliferation activities of **24** (**HFL1**, IC_{50} = 37.2 μM; **HPASMC**, IC_{50} = 22.4 μM), **31f** (**HFL1**, IC_{50} = 31.0 μM; **HPASMC**, IC_{50} = 20.3 μM) were roughly equivalent to **2** (**HFL1**, IC_{50} = 38.5 μM; **HPASMC**, IC_{50} = 17.0 μM). However, the vasodilatory effects of compounds **24** (EC_{50} = 0.96 μM) and **31f** (EC_{50} = 1.6 μM) displayed an obvious disadvantage compared to **2** (EC_{50} = 0.29 μM) which showed potent anti-proliferation activities and moderate vasodilatory effect. Taken together, compound **2** was selected as the best candidate for subsequent study.

The Vasodilatory Effect of 2 Through Stimulating sGC. sGC/cGMP signal transduction is crucial to vascular tone modulation in the pathogenesis of PAH. Pharmacological stimulation of sGC exerts intracellular effects by increasing the formation of cGMP that can be degraded by phosphodiesterase 5 (PDE-5). Because **2** was designed through introducing the pharmacophores of sGC stimulators based on the fragment design strategy, we expected that **2** could up-regulate the intracellular cGMP levels by activating sGC. Hence, **2** and riociguat were subjected to homogeneous time-resolved fluorescence (HTRF) cGMP assay to evaluate their effects on cGMP generation in HPASMCs. Firstly, in the absence of the PDE-5 inhibitor 3-isobutyl-1-methylxanthine (IBMX), **2** and riociguat slightly increased intracellular cGMP levels (about 5% increase at 100 μM, Figure 3A). Moreover, the presence or absence of sGC inhibitor 1*H*-[1,2,4]oxadiazolo [4,3-*a*] quinoxalin-1-one (ODQ) had no significant difference on the levels of cGMP (the red and blue lines shown in

Figure 3A). This is primarily due to the rapid cGMP degradation by the intracellular PDE-5. Secondly, with the addition of IBMX, we explored the impact of ODQ on cGMP formation in HPASMCs. As a result, **2** exhibited distinct ability to produce cGMP and showed a significant dose-dependent relationship, while the effect was moderate compared to riociguat (about 40% and 50% increase at 100 μM as the green and black lines shown in Figure 3B, respectively). In addition, the elevated levels of cGMP were obviously reduced after adding ODQ compared with the groups without ODQ (green vs red; black vs blue, Figure 3B). Taken together, these findings suggest that **2** was effective in elevating the intracellular cGMP levels possibly through stimulating sGC.

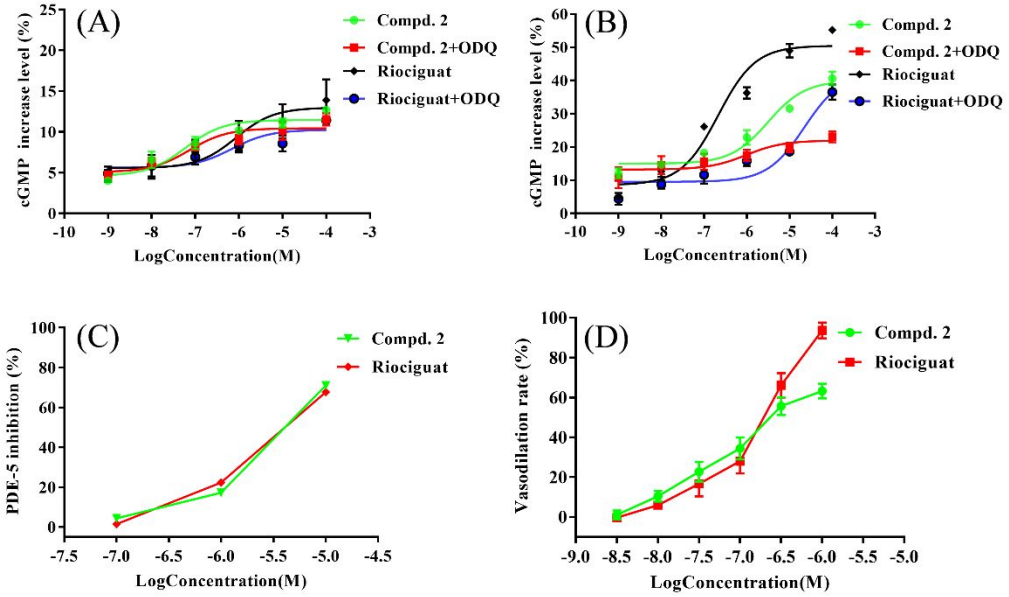

Figure 3. (A) Dose-dependent curve of compound **2** and riociguat to elevate the cGMP levels in the absence or presence of 10 μM ODQ in HPASMCs without IBMX, values are the average of three independent experiments. (B) Dose-dependent curve of compound **2** and riociguat to elevate the cGMP levels in the absence or presence of 10 μM ODQ in HPASMCs under condition of IBMX (10 μM), values are the average of three independent experiments. (C) The inhibition curve of compound **2** and riociguat on PDE-5. (D) Concentration-response curve of compound **2** and riociguat relaxing rat thoracic aorta rings. Value represent mean ± REM, $n = 3$.

As we noted above, stimulation of sGC promotes the production of cGMP, nevertheless, PDE-5 inhibition is also an alternative approach to elevate intracellular cGMP levels.[44] However, PDE-5 inhibitors do not stimulate the formation of cGMP, but inhibit its degradation in contrast to sGC stimulators which have a stronger effect on elevating cGMP levels. Herein, in order to validate whether the elevated cGMP after **2** treatment was induced via sGC stimulation rather than PDE-5 inhibition, we also tested the inhibitory effect of compound **2** against PDE-5 in this study.[45] The inhibition rate of compound **2** against PDE-5 at 100 nM was only 4.3%, while that of sildenafil at 2 nM was 54.9%. The results indicate that **2** exhibited a significantly weaker inhibitory effect on PDE-5 than the positive control sildenafil. In addition, **2** and riociguat showed comparable inhibitory potency against PDE-5 under different concentrations, as shown in Figure 3C. These data showed that compound **2** has little inhibitory effect on PDE-5, and its vasodilatory effect caused by cGMP elevation was achieved through stimulating sGC.

These results supported that compound **2** can noticeably activate sGC signaling pathway to relax blood vessels. In addition, the ability of **2** to elevate cGMP and lower blood pressure is milder than that of riociguat at high dosage, as illustrated in Figure 3B and Figure 3D. Furthermore, what sparked our enthusiasm for this work is that **2** exerted significantly potent anti-proliferation effects against HPASMCs and HLF1 compared with riociguat. Therefore, we speculated that the anti-proliferation effects of **2** may mainly through regulating AMPK signaling pathway.

The Vascular Remodeling Inhibition Effect of 2 via Mainly Regulating AMPK. Although the imbalance between pulmonary artery vasoconstriction and vasodilation contributes to the pathophysiology of the disease, the remodeling of pulmonary vascular represents the essential pathologic finding associated with PAH.[22, 23] Pulmonary vascular remodeling is characterized by

the thickening of pulmonary vessel wall. Such thickening is predominantly due to hyper-proliferation of smooth muscle cells and fibroblasts, such as HPASMCs and HLF1, respectively.[46, 47]

Interestingly, compound **2** significantly inhibited the over-proliferation against both HPASMCs (IC_{50} = 17.0 μM) and HLF1 (IC_{50} = 38.5 μM) induced by transforming growth factor β (TGF-β, 10 ng/mL) as discussed above. Recent studies reported that AMPK was up-regulated under the status of hypoxia, which is involved in inducing PASMCs proliferation as well as the formation of pulmonary vascular remodeling.[26, 48] Hence, we also investigated the anti-proliferation activity of **2** under hypoxic condition with compound C and riociguat as the positive controls. Results showed that **2** has the best IC_{50} values of 20.8 μM (HPASMCs, Figure 4A) and 34.9 μM (HLF1, Figure 4B), respectively. Accordingly, the dramatic anti-proliferation effects indicate that **2** may display significant advantages in inhibiting vascular remodeling compared to riociguat. In addition, the activities of compound C were stronger than that of riociguat against both HPASMCs (Figure 4A) and HLF1 (Figure 4B), indicating that inhibition of AMPK is more beneficial to inhibit cell proliferation than activation of sGC. Given the AMPK inhibitor compound C was also taken as a lead compound, and these data preliminarily support that compound **2** may exhibit anti-proliferation effects by inhibiting AMPK.

In order to investigate whether compound **2** inhibits AMPK, the inhibitory activity of **2** against AMPK was tested using HTRF assay. Here we showed that **2** inhibited AMPK activity in a dose-dependent manner consistent with compound C, while riociguat exerted no effect on AMPK (Figure 4C). Furthermore, **2** showed slightly weaker potency against the AMPK compared to compound C. According to the X-ray structural analysis of compound C, the pyrrazolo[1,5-*a*]-pyrimidine ring of

compound C is fixed in the corresponding region of AMPK and forms a hydrogen bond to Val96, and the pyrimidine ring forms a hydrogen bond with the water molecule (Figure 4D). However, docking analysis showed that **2** formed only one hydrogen bond between amino group and Val96 (Figure 4E).[34] Nevertheless, the computational docking mode led to identification that **2** binds to the pocket better than compound C, especially the binding of benzyl group to hydrophobic cavity. The results suggest that the activation of sGC after introducing benzyl moiety has little conflict with AMPK inhibition. Therefore, the significant anti-proliferation activities of **2** is most likely mediated by simultaneously regulating both AMPK and sGC pathways.

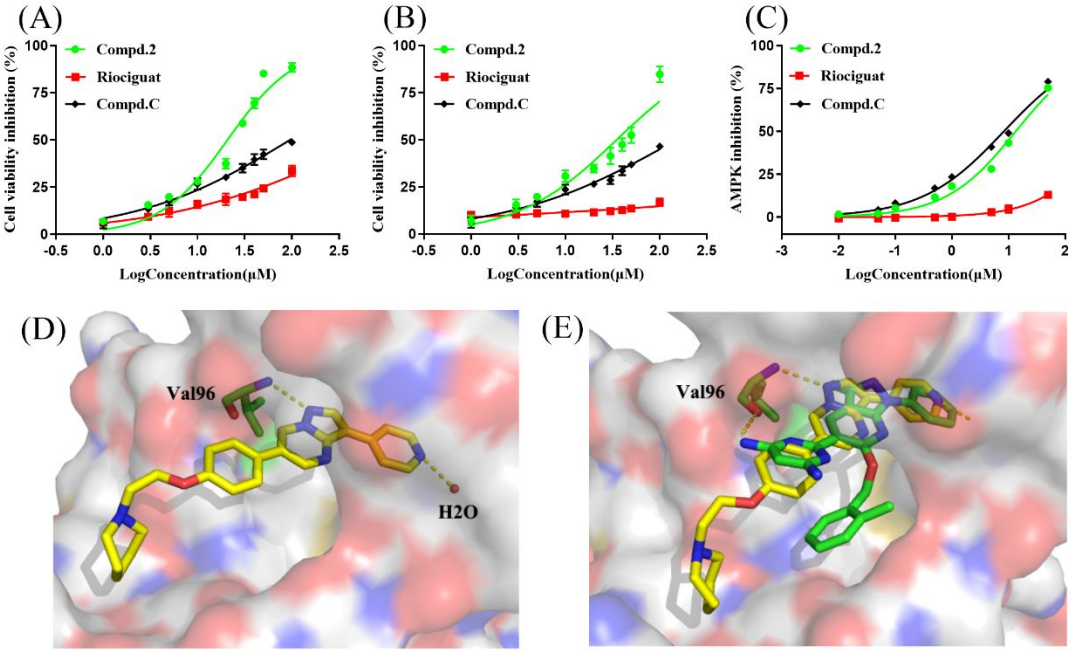

Figure 4. (A) Dose-dependent curve of **2**, riociguat and compound C to inhibit the proliferation of HPASMCs under hypoxic condition, values are the average of three independent experiments. (B) Dose-dependent curve of **2**, riociguat and compound C to inhibit the proliferation of HLF1 under hypoxic condition, values are the average of three independent experiments. (C) Dose-dependent curve of **2**, riociguat and compound C to inhibit AMPK, values are the average of three independent experiments. (D) Surface presentation of the compound C binding to the active site pocket of AMPK (PDB ID: 3aqv). (E) Surface presentation of **2** binding to the active site pocket of AMPK. **2**

and compound C are presented in colors of green and yellow, respectively. Atoms of carbon, nitrogen, and oxygen of AMPK are presented in colors of white, blue, and red, respectively. Hydrogen bonds are indicated with yellow dashed lines.

As previously mentioned, the abnormal migration of HPASMCs and HLF1 plays a pivotal role in vascular remodeling. To further explore whether **2** regulates the migration of HPASMCs and HLF1, scratch assay was used to detect the migratory activity after **2** treatment with the compound C and riociguat as comparisons. We synchronously investigated the effects of these compounds with different concentrations and induction conditions against cell lines migration. The effects of compound **2** to inhibit cells migration are shown in Figure 5. Compared with the control group, cell migration was significantly increased in the model group ($p < 0.01$). These results suggest that **2** showed greatest potency among the tested 3 compounds in a dose-dependent manner, which is consistent with the anti-proliferation activity. In addition, compounds are more sensitive to suppress HPASMCs migration under the condition of hypoxia (Figure 5A, B), while the suppression of HLF1 migration are more effective in the presence of TGF-β (Figure 5C, D). In a word, **2** remarkably suppressed cell migration against both HPASMCs and HLF1, which play a key role in pulmonary vascular remodeling, especially against HPASMCs under hypoxic condition.

These data suggest that **2** exhibited remarkable proliferation and migration suppression effects mainly mediated by AMPK pathway inhibition. Moreover, both effects can also be enhanced synergistically through upregulation of cGMP level via moderately stimulating sGC, indicating that **2** will show significant advantages in inhibiting vascular remodeling *in vivo.*

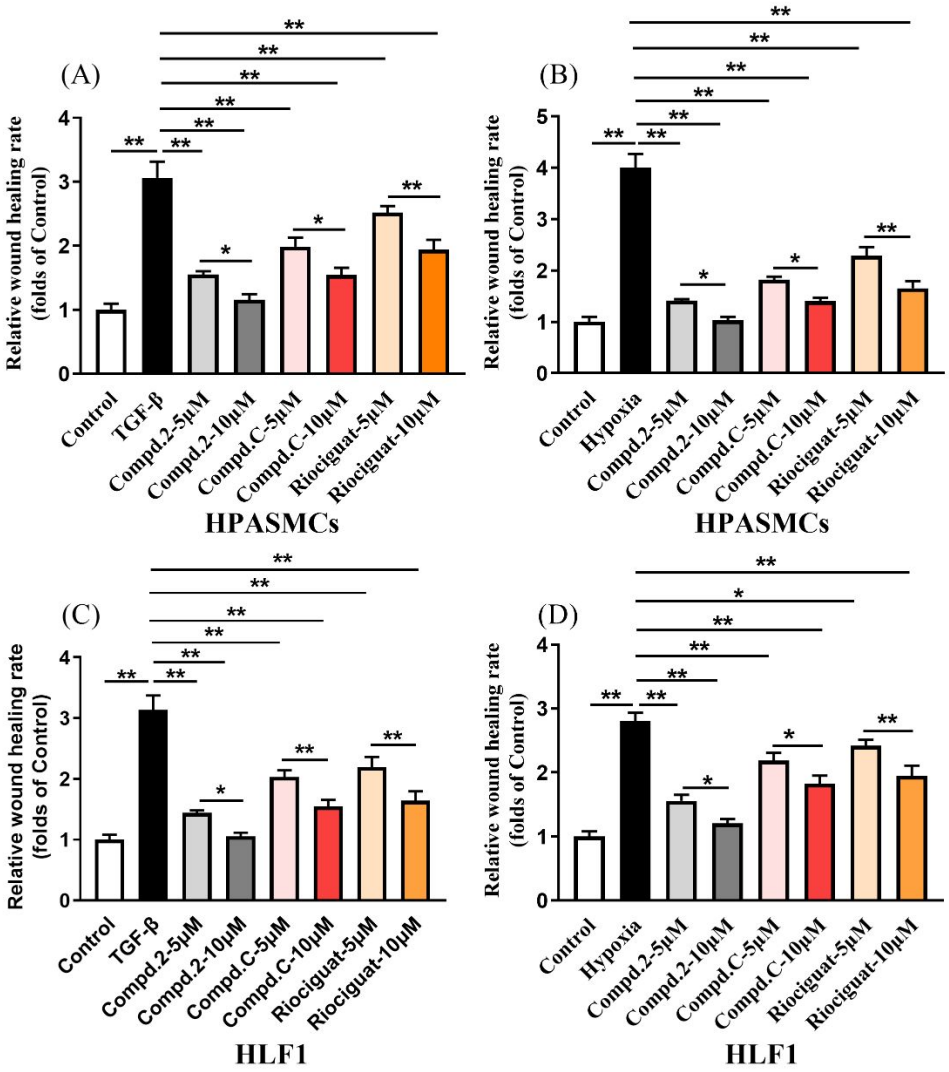

Figure 5. Effects of **2** on inhibiting vascular cells migration. Movement of cells into wound was shown for cells at 0 and 24 h. (A) Effects of **2**, riociguat and compound C inhibit HPASMCs migration induced by TGF-β (10 ng/mL). (B) Effects of **2**, riociguat and compound C inhibit HPASMCs migration under hypoxic condition (C) Effects of **2**, riociguat and compound C inhibit HLF1 migration induced by TGF-β (10 ng/mL). (D) Effects of **2**, riociguat and compound C inhibit HLF1 migration under hypoxic condition. Data were shown as the mean ± SD from three independent experiments. (∗) $p < 0.05$, (∗∗) $p < 0.01$.

Reasonable Physicochemical Properties to Enable *in vivo* Studies. To further characterize the physicochemical properties (Table 2) of compound **2**, its water solubility, metabolic stability and plasma protein binding rate were evaluated. As is well-known that liver microsomes (human and

rat) are extensively used to perform *in vitro* drug metabolism assays. Herein, compound **2** was subjected to metabolic stability evaluation by human and rat liver microsomal experiments *in vitro*. The results indicate that **2** was more stable in human liver microsome ($t_{1/2}$ of 125 min, and Cl_{int} of 14 mL/min/mg, respectively) than that in rat liver microsome ($t_{1/2}$ of 10 min, and Cl_{int} of 248 mL/min/mg, respectively). This difference may be caused by species differences or individual differences. The plasma protein binding rate of **2** in human (99.8%) and rat (99.3%) was comparable to the positive control warfarin (98.9% and 99.4%). Compound **2** could be a starting point for a new strategy in treating PAH although its drug-like properties are limited at the current stage, which needs further study in the next logic step.

Table 2. Physicochemical Properties of Compound 2

Content	Value
Water solubility (pH: 7.3)	34 ng/mL
Water solubility (pH: 3.5)	28 μg/mL
Human liver microsome stability ($T_{1/2}$)	125 min
Rat liver microsome stability ($T_{1/2}$)	10 min
Human liver microsome stability (Cl_{int})	14 mL/min/mg
Rat liver microsome stability (Cl_{int})	248 mL/min/mg
Human plasma binding rate	99.8 %
Rat plasma binding rate	99.3 %

In Vivo Notable Therapeutic Effects of 2 in PAH Rat Models. To investigate the pharmacodynamics of compound **2**, a PAH rat model was established using hypoxia method.[49, 50] Compound **2** and riociguat at equimolar dose (10 mg/kg) were orally administrated daily for 2 weeks

under hypoxia after hypoxia-induced PAH rat model has been built in the first 2 weeks. In keeping with previous studies, RVSP was significantly increased in the hypoxia model group (26.2 mmHg) compared with the normoxic group (16.2 mmHg, $p < 0.01$). This result suggested successful PAH rat models after 4 weeks of exposure to hypoxic condition. After treatment, a significant decrease of RVSP was measured in the groups treated with **2** (22 mmHg) and riociguat (22.3 mmHg) compared to that of the hypoxia group (26.2 mmHg) (Figure 6A) at a dose of 10 mg/kg ($p < 0.01$). Although the effects of **2** on increasing cGMP in HPASMCs and relaxing rat aortic ring were lower than that of riociguat, its ability to reduce right ventricular pressure *in vivo* was comparable to that of riociguat, suggesting that the vascular remodeling inhibition effect of **2** plays a pivotal role in the treatment of PAH.

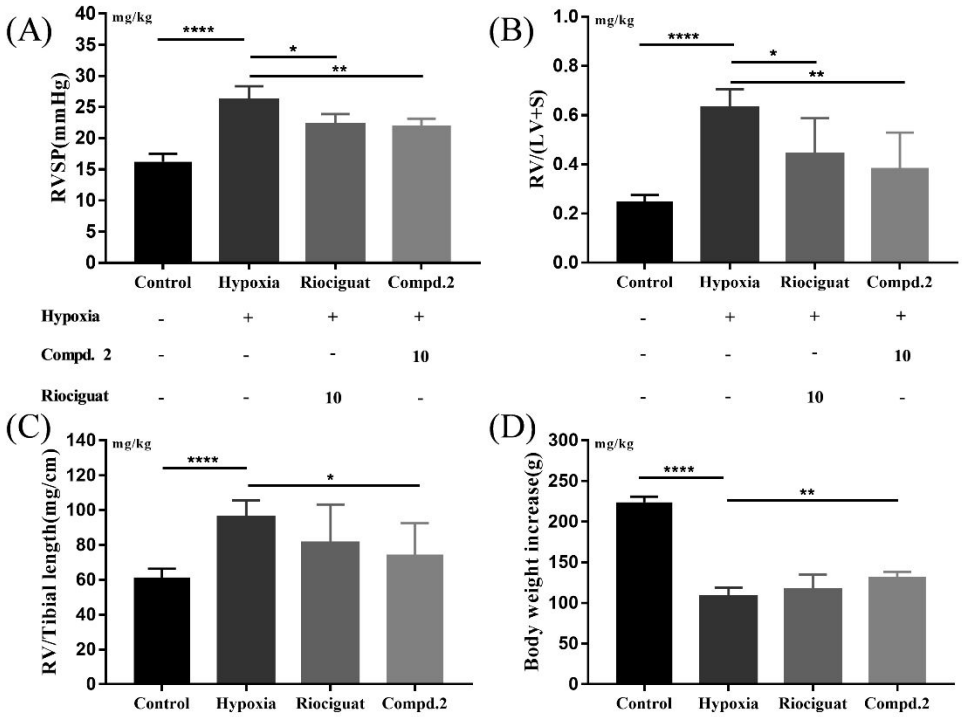

Figure 6. Effects of **2** and riociguat in hypoxia treated rats. The hypoxia-induced PAH rats were orally treated daily with **2** and riociguat at a dose of 10 mg/kg for two weeks. (A) Effects of **2** and riociguat on RVSP of the rats. (B) Effects of **2** and riociguat on RV/ (LV + S) of the rats. (C) Effects of **2** and riociguat on RV/tibial length of the rats.

(D) Effects of **2** and riociguat on body weight change of the rats. These data are indicated as the mean ± SEM (n = 5/group). (∗) $p < 0.05$, (∗∗) $p < 0.01$.

The effects of **2** on the RVH are shown in Figure 6. The weight ratio of right ventricle /left ventricle + septum [RV/(LV+S), Figure 6B] was used to indicate RVH and ratio of RV/tibial length (Figure 6C) was also measured, the model group [RV/(LV+S) = 0.63] showed significant increase than the control group ($p < 0.01$). Notably, oral administration of **2** (10 mg/kg) daily for 14 days dramatically reduced RV/(LV+S) (0.38), which was superior to riociguat [RV/(LV+S) = 0.44]. Similar trends were also observed in RV/tibial length and body weight change (Figure 6D).

2 Significantly Ameliorates Pulmonary Vascular Remodeling of PAH Rats. Elevated pulmonary vascular remodeling presents the hallmarks of PAH, such as increased PAMT and aberrant pulmonary vascular fibrosis.[51] In order to investigate the effect of compound **2** on vascular remodeling, hematoxylin and eosin (H&E) was used to stain the lung tissues. As shown in Figure 7A and Figure 7B, PAMT was thickened in hypoxia-induced PAH rats in contrast to the control group, which was remarkably reduced after **2** and riociguat treatment. Moreover, the therapeutic effect of **2** was more prominent than that of riociguat.

It is well-known that TGF-β plays a key role in the pathogenesis of fibrotic diseases and is also involved in PAH development.[52] Furthermore, increased TGF-β expression contributes to vascular remodeling in the progress of PAH.[53] Accordingly, we performed Western blotting analysis to test the effects of **2** and riociguat on TGF-β level. Our results indicated that **2** significantly downregulated hypoxia-induced the over-expression of TGF-β in lung tissues (Figure 7C and Figure 7D). To address whether compound **2** mediates the process of fibrosis via canonical TGF-β signaling

pathways during hypoxia-induced PAH, we next determined the levels of total Smad2/3 (t-Smad2/3) and phosphorylated Smad2 (p-Smad2). Consistently, hypoxia significantly induced the levels of p-Smad2 without statistically altering t-Smad2/3 levels compared with the control group. Treatment with **2** (10 mg/kg) did not change levels of t-Smad2/3, however, abolished the over-phosphorylation of Smad2, which agrees with the effect on TGF-β (Figure 7C).

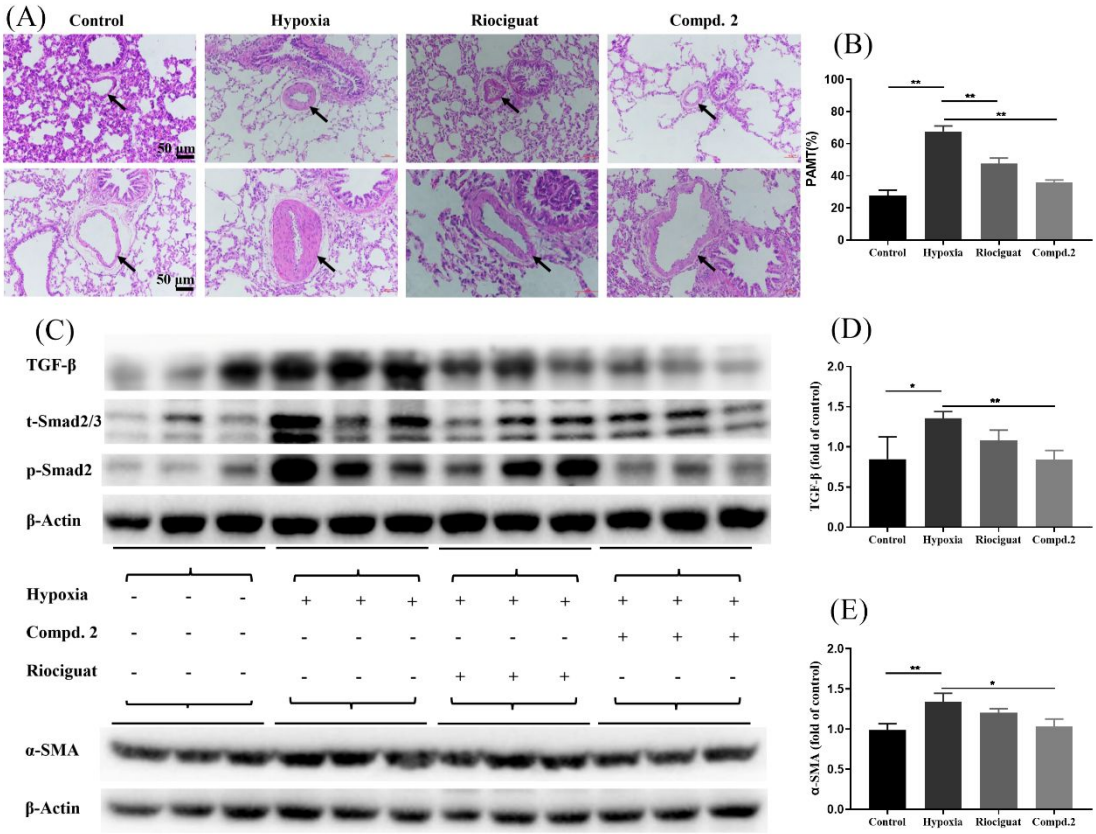

Figure 7. Effects of **2** and riociguat on attenuating pulmonary vascular remodeling of rats with PAH. (A) Representative images of pulmonary vascular in the lungs by H&E staining for morphology. Scale bar at the lower right corner = 50 μm. (B) The PAMT quantifications in the lungs. **2** (10 mg/kg) markedly lowered hypoxia-induced pulmonary artery medial thickness (n = 5/group). (C) Representative images of TGF-β, Smad2/3 and α-SMA in the lungs by western blotting. **2** markedly reduced hypoxia-induced over-expression of TGF-β, p-Smad2 and α-SMA in the lungs. (D) The quantitative ratio of TGF-β to β-actin in the lungs. (E) Quantification of ratio of α-SMA to β-actin in the lungs. The tests were independently performed for three times. The data are reported as the mean ± SEM

(n = 3/group). (∗) $p < 0.05$, (∗∗) $p < 0.01$.

Studies have shown that α-smooth muscle actin (α-SMA) is the marker of muscularization, and its over-expression could mainly contribute to structural changes in PAH.[54] Therefore, the effect of **2** on this marker were evaluated via Western blotting analysis. As expected, **2** significantly attenuated hypoxia-induced up-expression of α-SMA compared to riociguat (Figure 7C, E).

2 Regulated both sGC and AMPK Signaling Pathways against PAH in Rats. To address whether **2** inhibits hypoxia-induced PAH via sGC stimulation and AMPK inhibition, we measured the levels of related proteins downstream of these two pathways. Protein kinases G (PKG) have been characterized as crucial downstream mediators of sGC/cGMP in the regulation of vascular tone and remodeling.[55, 56] Vasodilator-stimulated phosphoprotein (VASP) is a prime substrate of PKG, and its activity is commonly assessed by phosphorylation levels of VASP at Ser239 (p-VASP).[57] Recent data showed that downregulation of sGC leads to reduced levels of cGMP and impaired PKG activity with decreased levels of p-VASP, whereas the levels of PKG1 are increased in a compensatory manner to make up for the damaged sGC-cGMP-PKG activity.[56] As shown in Figure 8A and Figure 8B, **2** observably attenuated the compensatory expression of PKG1 in contrast to the levels of p-VASP, which in accordance with the effects of elevating cGMP in HPASMCs. Hence, these results further demonstrated that **2** could protect against the development of hypoxia-induced PAH via sGC stimulation although at lower level than that of riociguat.

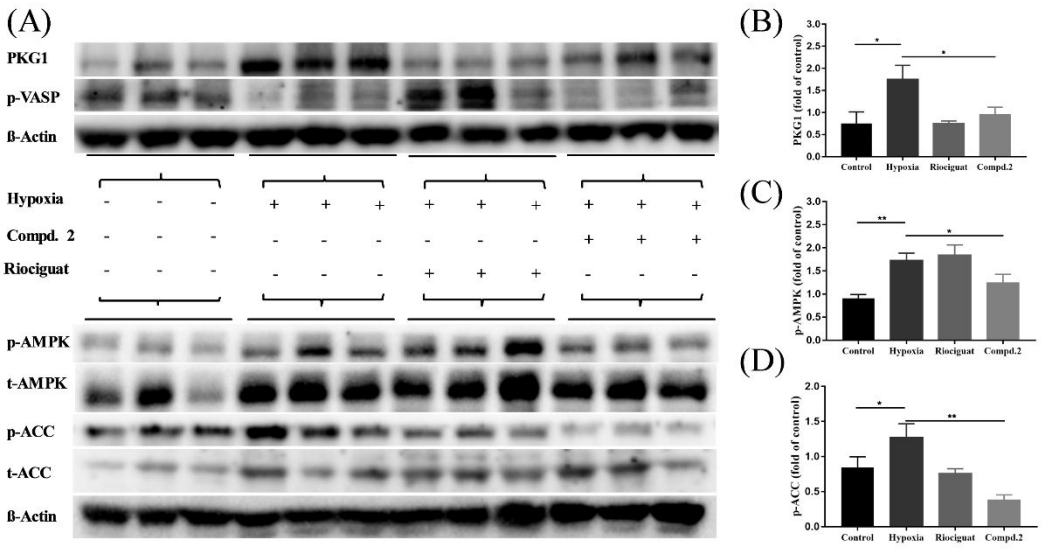

Figure 8. Effects of **2** on regulating sGC and AMPK dual signaling pathways. (A) Representative images of Western blotting for PKG1, p-VASP, p-AMPK, t-AMPK, p-ACC and t-ACC in hypoxia-induced PAH rat lungs. **2** significantly decreased hypoxia-induced over-expression of PKG1, p-AMPK and p-ACC in the lungs. (B) Quantification of ratio of PKG1 to β-actin. (C) Quantification of ratio of p-AMPK to β-actin. (D) Quantification of ratio of p-ACC to β-actin in the lungs. The tests were independently performed for three times. The data are reported as the mean ± SEM (n = 3/group). (∗) $p < 0.05$, (∗∗) $p < 0.01$.

In addition, it was reported that AMPK is a key player in the hypoxia-induced PAH, which results in increased phosphorylation of AMPK and ACC, a downstream target and standard reporter for AMPK activity.[23] Thus, we investigated whether compound **2** acts through AMPK pathway inhibition. Treatment with **2** significantly decreased the phosphorylation levels of AMPK and ACC without changing total levels of AMPK and ACC in hypoxia-induced PAH rat lungs (Figure 8A, C, D). These results suggest that **2** could prevent PAH development by inhibiting AMPK signaling pathway. Taken together, **2** is more efficient in treating PAH through simultaneous regulation of sGC and AMPK dual pathways, especially through its anti-vascular remodeling profiles.

In summary, compound **2** significantly inhibited HPASMCs and HLF1 proliferation and migration mainly by inhibiting AMPK, as well as relaxing vascular vessels via stimulating sGC *in vitro*. Moreover, **2** remarkably decreased RVSP, RVH, PAMT and pulmonary vascular remodeling *in vivo* even though the moderate vasodilatory effect compared to riociguat, indicating the enormous advantages of **2** with dual activities of vascular remodeling inhibition and vasodilation. Furthermore, **2** exhibited highlighted anti-vascular remodeling effect and prominently prevented the progression of tissue fibrosis. These data suggest that with the potent and valuable anti-vascular remodeling activity, **2** significantly improved the vascular pathological characteristics in PAH compared to the reference compound riociguat.

As the essential pathological characteristic of PAH, vascular remodeling has been paid more and more attention in the field of anti-PAH drug discovery. The abnormal phenotypes in pulmonary vascular cells under PAH result in vasoconstriction and loss of elasticity of vascular wall, which will eventually contribute to increased PAP, RVH and right ventricular overload. Clinically, high PAP is the primary symptom to be dealt with, which is the major strategy for current therapy, i.e. diuretics, calcium channel blockers, anticoagulants, inhaled NO donors, and targeted therapy including NO pathway regulators (sGC stimulators or PDE-5 inhibitors), endothelin receptor antagonists and prostacyclin analogs. However, this kind of "symptom-based" strategy is gradually running into drawbacks and bottlenecks such as drug resistance, systematic hypotension and unsatisfactory long-term use due to less consideration of the essential pathological characteristics of PAH. As a result, agents with dual regulatory activities on vascular remodeling and vasodilation will show potential advantages in long-term outcomes and achievements of predefined treatment goals. This will also contribute to the strategy switch from "symptom-based" to "pathology-based"

in PAH treatment.

CONCLUSION

In this study, compound **1** was initially designed and synthesized with riociguat and compound C as the lead compounds based on fragment-guided drug discovery strategy. Subsequently, we designed, synthesized and evaluated a series of novel pyrazolo[3,4-*b*] pyridine derivatives with dual effects of pre-constricted rat thoracic aorta rings and cell viability based on the structure of **1**. Compared with riociguat, **2** displayed moderate vasodilatory effect and significant improved inhibitory activities against HPASMCs and HLF1 proliferation and migration *in vitro*. More importantly, **2** significantly decreased RVSP, myocardial and vascular remodeling (RVH and PAMT) via moderate regulatory effect on sGC/cGMP pathway and considerable inhibition against AMPK signaling pathway *in vivo*. In conclusion, the results in this study demonstrated that agents characterized by higher anti-vascular remodeling potency and moderate vasodilation effect will show more advantages in PAH treatment. **2** could be further evaluated as a potential lead for anti-PAH drug discovery based on "pathology-based" strategy through regulating dual functions of vascular remodeling and vasodilation instead of mono vasodilation function in "symptom-based" strategy.

EXPERIMENTAL SECTION

General Chemical Methods. Unless otherwise indicated, all starting materials and reagents were purchased from standard suppliers (Sigma-Aldrich, Aladdin, Energy Chemical, Shanghai bide) and used directly without further purification. Melting point was determined on a XT4MP melting apparatus (Taike Co., LTD). NOVA-2S microwave apparatus (Preekem, Yiyao technology co.,

LTD) was used for microwave reaction. Column chromatography purification was carried out on silica gel (80-100 mesh and 200-300 mesh). All reactions were monitored by Thin layer chromatography (TLC) on 0.25 mm glass-backed silica gel plates (silica GF-254), and visualized with ultraviolet (UV) light (254 nm). Anhydrous reaction conditions were performed under argon. The purity of all target compounds was confirmed to be > 95% by HPLC which was carried out at room temperature using a Welchrom C18 (250 × 4.6 mm, 5 μm) in a speed of 1.0 mL/min with methanol and ammonium acetate in water (0.05 mol/L, 65%-85%, v/v) as mobile phase under 254 nm wavelength. The ^{1}H NMR and ^{13}C NMR and 2D-HMBC spectra were recorded at room temperature on a Bruker AVANCE III 500 MHz and 400 MH_Z spectrometer with tetramethylsilane (TMS) as an internal standard. Chemical shifts are expressed in parts per million (ppm) relative to TMS (ppm = 0.00). The coupling constants are reported in Hz. Peak multiplicity abbreviations are as follows: s (singlet), d (doublet), dd (two doublets), t (triplet), q (quartet), br s (broad singlet), and m (multiplet). HRMS were performed on a Finnigan MAT95 mass spectrometer.

5-Chloro-3-methyl-1-phenyl-1H-pyrazole-4-carbaldehyde (4). To a solution of phosphorus oxychloride (53 mL, 574 mmol) in *N,N*-dimethylformamide (DMF, 35 mL) at 0 °C for 10 min. Then the mixture was added to 5-methyl-2-phenyl-2,4-dihydro -3*H*-pyrazol-3-one (**3**) (25 g, 143 mmol) at room temperature. The mixture was stirred at 100 °C for 2 h. After the solution had cooled to room temperature, it was poured into a mixture of ice and water (1000 mL), then light yellow solid was formed, which was filtered to afford crude filter cake (30.5 g). The filtrate was extracted with dichloromethane (DCM, 3 × 200 mL). The combined organic extracts were dried over anhydrous sodium sulfate and concentrated, which was purified combined with crude filter cake by silica gel column chromatography (petroleum ether/EtOAc, 5:1) to get the product **4** (27.8 g) as a white solid.

Yield: 90%. Purity: 99%. ^{1}H NMR (500 MHz, DMSO-d_6): δ 9.64 (s, 1H), 7.62-7.38 (m, 5H), 2.54 (s, 3H). ^{13}C NMR (126 MHz, DMSO-d_6): δ 183.74, 151.37, 137.04, 133.29, 129.27 × 2, 129.18, 125.20 × 2, 117.45, 13.76. HRMS (ESI) *m/z* calcd $C_{11}H_9ClN_2O^+$ $[M + H]^+$: 221.0403, found 221.0914, error 231.2 ppm.

5-azido-3-methyl-1-phenyl-1H-pyrazole-4-carbaldehyde (5). To a solution of **4** (20 g, 91 mmol) in dimethylsulfoxide (DMSO-d_6, 150 mL) were added tetrabutyl ammonium iodide (4.03 g, 10.9 mmol) and sodium azide (7.09 g, 109 mmol). The mixture was stirred at room temperature for 18 h until the start material disappeared as monitored by TLC. Then it was poured into a mixture of ice and water (500 mL). The resulting solution was extracted with portions of ethyl acetate (2 × 300 mL). The combined organic extracts were washed with brine (2 × 200 mL) and dried over anhydrous sodium sulfate. Then the organic layer was filtered and the filtrate was concentrated to give a crude, which was purified by silica gel column chromatography (petroleum ether/EtOAc, 6:1) to get the product **5** (19.25 g) as a light yellow solid. Yield: 93%. Purity: 99%. ^{1}H NMR (500 MHz, DMSO-d_6): δ 9.68 (s, 1H), 8.09 - 7.01 (m, 5H), 2.48 (s, 3H). ^{13}C NMR (126 MHz, DMSO-d_6): δ 183.62, 152.07, 137.02, 133.12, 129.11 × 2, 128.56, 124.28 × 2, 112.33, 12.72. HRMS (ESI) *m/z* calcd $C_{11}H_9N_5O^+$ $[M + H]^+$: 228.0841, found 228.0743, error -43.0 ppm.

5-amino-3-methyl-1-phenyl-1H-pyrazole-4-carbaldehyde (6). To a solution of **5** in ethyl acetate (100 mL) were added ammonium chloride (23.6 g, 441 mmol) in water (100 mL) and iron powder (14.7 g, 264 mmol) at room temperature. The mixture was stirred at room temperature for 22 h until **5** was consumed completely as monitored by TLC. The mixture was filtered on diatomite and the filtrate was extracted with ethyl acetate (3 × 300 mL). The combined organic layer was washed with saturated aqueous sodium bicarbonate (2 × 200 mL) and dried over anhydrous sodium sulfate, and

then evaporated under vacuum to afford a residue, which was purified by silica gel column chromatography (petroleum ether/EtOAc, 3:1) to provide the product **6** (19.25 g) as a white solid. Yield: 9%. Purity: 99%. ^{1}H NMR (500 MHz, $CDCl_3$): δ 9.71 (s, 1H), 7.53-7.49 (m, 4H), 7.43-7.38 (m, 1H), 5.88 (s, 2H), 2.42 (s, 3H). ^{13}C NMR (126 MHz, DMSO-d_6): δ 183.93, 150.74, 149.25, 136.90, 129.84 × 2, 128.17, 123.68 × 2, 105.72, 11.19. HRMS (ESI) *m/z* calcd $C_{11}H_{11}N_3O^+$ [M + H]$^+$: 202.0936, found 202.0843, error -46.0 ppm.

5-((2-fluorobenzyl)amino)-3-methyl-1-phenyl-1H-pyrazole-4-carbaldehyde (7). To a solution of **6** (35 g, 174 mmol) in acetonitrile (CH_3CN, 200 mL) were added anhydrous potassium carbonate (60 g, 435 mmol) and 1-(bromomethyl)-2- fluorobenzene (28 mL, 233 mmol) at room temperature. The reaction was completed after the mixture was stirred at room temperature for 8 h monitoring by TLC. The suspension was filtered and the filtrate was concentrated under reduced pressure to provide a crude, which was purified by silica gel column chromatography (petroleum ether/EtOAc, 10:1 to 5:1) to afford the product **7** (29.6 g) as a white solid. Yield: 55%. Purity: 99%. ^{1}H NMR (500 MHz, DMSO-d_6): δ 9.63 (s, 1H), 7.50-7.43 (m, 4H), 7.41-7.36 (m, 2H), 7.30-7.25 (m, 1H), 7.15-7.05 (m, 3H), 4.29 (d, J = 6.9 *Hz*, 2H), 2.28 (s, 3H). ^{13}C NMR (126 MHz, DMSO-d_6): δ 183.75, 160.28, 150.85, 150.69, 138.79, 129.67 × 2, 129.66, 129.14, 128.91, 125.99 × 2, 125.86, 124.83, 115.50, 106.98, 42.09, 12.73. HRMS (ESI) *m/z* calcd $C_{18}H_{16}FN_3O^+$ [M + H]$^+$: 310.1277, found 310.1360, error 26.8 ppm.

General Procedure for the Synthesis of 8 and 11.

7-(2-fluorobenzyl)-3-methyl-6-oxo-1-phenyl-6,7-dihydro-1H-pyrazolo[3,4-b]pyridine-5-carbonitrile (8). To a solution of **7** (28 g, 90.6 mmol) in acetic acid was added ethyl cyanoacetate (30 mL, 281 mmol) at room temperature. The mixture was refluxed for 72 h monitoring by TLC.

After the residue was cooled to room temperature, the solvent was removed by vacuum distillation. The solid was purified by recrystallization from ethyl alcohol and the filtrate was purified by silica gel column chromatography (petroleum ether/EtOAc, 15:1) to provide **8** (17.6 g, 49.2 mmol) combined two batches as light yellow solid. Yield: 54%. Purity: 97.7%. ^{1}H NMR (500 MHz, DMSO-d_6): δ 8.89 (s, 1H), 7.47-7.43 (m, 1H), 7.29-7.17 (m,5H), 7.05 (t, J = 7.6 *Hz*, 1H), 6.96 (dd, J = 9.9, 8.5 *Hz*, 1H), 6.72 (t, J = 7.3 *Hz*, 1H), 5.02 (s, 2H), 2.41 (s, 3H). ^{13}C NMR (126 MHz, DMSO-d_6): δ 160.72, 159.75, 146.21, 143.90, 143.14, 137.98, 130.44, 129.65, 129.14 × 2, 128.15 × 2, 127.28, 124.83, 122.10, 117.35, 115.46, 106.58, 96.49, 41.30, 11.69. HRMS (ESI) *m/z* calcd $C_{21}H_{15}FN_4O^+$ $[M + H]^+$: 359.1230, found 359.1318, error 24.5 ppm.

3-methyl-6-oxo-1-phenyl-6,7-dihydro-1H-pyrazolo[3,4-b]pyridine-5-carbonitrile (11 or 12b). Compound **11** was prepared in 70% yield from **6** and ethyl cyanoacetate following a similar procedure to that described for synthesis of **8**. ^{1}H NMR (500MHz, DMSO-d_6): δ 12.43 (s, 1H), 8.32-8.26 (m, J = 9.1 Hz, 2H), 7.95 (s, 1H), 7.41-7.37 (m, 2H), 7.13-7.10 (m, 1H), 2.31 (s, 3H). ^{13}C NMR (126MHz, DMSO-d_6): δ 169.84, 155.81, 143.64, 140.92, 136.49, 128.91 × 2, 119.37 × 2, 121.75, 119.31, 105.06, 95.22, 12.36. HRMS (ESI) *m/z* calcd $C_{14}H_{10}N_4O^+$ $[M + H]^+$: 251.0888, found 251.0925, error 14.7 ppm.

General Procedure for the Synthesis of 12a-i.

6-((2-fluorobenzyl)oxy)-3-methyl-1 -phenyl-1H-pyrazolo[3,4-b]pyridine-5-carbonitrile (12a). To a solution of **11** (30 g, 120 mmol) in DMF was added anhydrous potassium carbonate (20 g, 145 mmol) and 1-(bromomethyl)-2-fluorobenzene (15.9 mL, 132 mmol) at room temperature. The mixture was stirred at room temperature for 4 h until **11** disappeared as monitor by TLC. After the mixture was cooled to room temperature, it was poured into a mixture of ice and water (1000 mL),

then white solid was formed which was filtered to afford crude filter cake (40 g). The crude solid was recrystallized in CH_3CN (200 mL). The suspension was filtered to afford filter cake (35 g) and the filtrate was purified by silica gel column chromatography (petroleum ether/EtOAc, 5:1) to provide **12a** (36.6 g, 102 mmol) combined two batches as white solid. Yield: 85%. Purity: 98%. ^{1}H NMR (400 MHz, $CDCl_3$): δ 8.25 (s, 1H), 8.13-8.11 (m, *J* = 7.7 *Hz*, 2H), 7.60-7.50 (m, 3H), 7.34-7.29 (m, 2H), 7.25-6.96 (m, 2H), 5.66 (s, 2H), 2.60 (s, 3H). ^{13}C NMR (101 MHz, $CDCl_3$): δ 162.36, 161.83, 159.41, 148.96, 144.09, 138.58, 137.78, 130.02, 129.77, 128.96 × 2, 126.48, 124.33, 122.85, 120.76 × 2, 115.53, 115.32, 112.08, 91.71, 63.20, 12.45. HRMS (ESI) *m/z* calcd $C_{21}H_{15}FN_4O^+$ [M + H]$^+$: 359.1263, found 359.0907, error -99.1 ppm.

6-((3-Fluorobenzyl)oxy)-3-methyl-1-phenyl-1H-pyrazolo[3,4-b]pyridine-5-carbonitrile (12c). Compound **12c** was prepared in 89% yield from **11** and ethyl cyanoacetate following a similar procedure to that described for synthesis of **12a**. Purity: 99%.^{1}H NMR (400 MHz, $CDCl_3$): δ 8.22 (s, 1H), 8.07-8.10 (m, *J* = 7.5 *Hz*, 2H), 7.58-7.51 (m, 3H), 7.37-7.30 (m, 1H), 7.21-7.07 (m, 2H), 7.02-6.97 (m, 1H), 5.60(s, 2H), 2.57 (s, 3H). ^{13}C NMR (101 MHz, $CDCl_3$): δ 162.36, 161.83, 159.41, 148.96, 144.09, 138.58, 137.78, 130.02, 129.75, 129.06 × 2, 126.29, 124.50, 123.32, 120.84 × 2, 115.62, 115.37, 111.96, 91.79, 66.16, 12.42. HRMS (ESI) *m/z* calcd $C_{21}H_{15}FN_4O^+$ [M + H]$^+$: 359.1263, found 359.0907, error -99.1 ppm.

6-((4-Fluorobenzyl)oxy)-3-methyl-1-phenyl-1H-pyrazolo[3,4-b]pyridine-5-carbonitrile (12d). Compound **12d** was prepared in 76% yield from **11** and ethyl cyanoacetate following a similar procedure to that described for synthesis of **12a**. Purity: 96%. ^{1}H NMR (400 MHz, $CDCl_3$): δ 8.24 (s, 1H), 8.10 (m, *J* = 9.5 *Hz*, 2H), 7.55-7.49 (m, *J* = 19.6, 11.0 Hz, 4H), 7.38-7.35 (m, 1H), 7.10-7.07 (m, *J* = 17.3 *Hz*, 2H-), 5.54 (s, 2H), 2.59 (s, 3H). ^{13}C NMR (101 MHz, $CDCl_3$): δ 164.15,

161.06, 160.78, 149.04, 144.12, 138.34, 137.73, 131.69, 129.81, 129.75, 129.08 × 2, 126.43, 120.95 × 2, 115.80, 115.60, 115.43, 111.87, 91.77, 68.67, 12.43. HRMS (ESI) *m/z* calcd $C_{21}H_{15}FN_4O^+$ [M + H]$^+$: 359.1263, found 359.0907, error -99.1 ppm.

3-Methyl-6-((3-methylbenzyl)oxy)-1-phenyl-1H-pyrazolo[3,4-b]pyridine-5-carbonitrile (12e). Compound **12e** was prepared in 90% yield from **11** and ethyl cyanoacetate following a similar procedure to that described for synthesis of **12a**. Purity: 98%. ^{1}H NMR (400 MHz, $CDCl_3$): δ 8.30 (s, 1H), 8.23-8.12 (m, *J* = 8.6, 1.0 *Hz*, 2H), 7.61-7.58 (m, 2H), 7.34-7.22 (m, *J* = 8.0 *Hz*, 2H), 7.37-7.34 (m, *J* = 7.4 *Hz*, 1H), 7.28-7.22 (m, 2H), 5.58 (s, 2H), 2.63 (s, 3H), 2.39 (s, 3H). ^{13}C NMR (101 MHz, $CDCl_3$): δ 163.23, 148.93, 144.27, 138.64, 138.10, 137.76, 132.72, 129.27 × 2, 129.06 × 2, 127.97 × 2, 126.33, 120.95 × 2, 115.92, 112.09, 91.65, 66.01, 21.25, 12.47. HRMS (ESI) *m/z* calcd $C_{22}H_{18}N_4O^+$ [M + H]$^+$: 355.1514, found 355.1549, error 9.9 ppm.

3-Methyl-6-((2-methylbenzyl)oxy)-1-phenyl-1H-pyrazolo[3,4-b]pyridine-5-carbonitrile (12f). Compound **12f** was prepared in 88% yield from **11** and ethyl cyanoacetate following a similar procedure to that described for synthesis of **12a**. Purity: 98%.^{1}H NMR (400 MHz, $CDCl_3$): δ 8.28 (s, 1H), 8.27-8.14 (m, *J* = 7.7 *Hz*, 2H), 7.60-7.55 (m, 3H), 7.38-7.31 (m, 1H), 7.31-7.17 (m, 2H), 7.05-6.95 (m, 1H), 5.59(s, 2H), 2.61 (s, 3H) 2.37 (s, 3H). ^{13}C NMR (101 MHz, $CDCl_3$): δ 163.36, 148.83, 144.41, 138.96, 138.09, 137.58, 133.78, 130.02 × 2, 129.75 × 2, 129.06 × 2, 126.29, 120.84 × 2, 115.82, 112.37, 91.79, 66.16, 21.32, 12.42. HRMS (ESI) *m/z* calcd $C_{22}H_{18}N_4O^+$ [M + H]$^+$: 355.1514, found 355.1549, error 9.9 ppm.

3-Methyl-6-((4-methylbenzyl)oxy)-1-phenyl-1H-pyrazolo[3,4-b]pyridine-5-carbonitrile (12g). Compound **12g** was prepared in 88% yield from **11** and ethyl cyanoacetate following a similar procedure to that described for synthesis of **12a**. Purity: 99%.^{1}H NMR (400 MHz, $CDCl_3$): δ 8.27

(s, 1H), 8.23-8.10 (m, *J* = 8.6, 1.0 *Hz*, 2H), 7.59-7.50 (m, 2H), 7.44-7.42 (m, *J* = 8.0 *Hz*, 2H), 7.38-7.34 (m, *J* = 7.4 *Hz*, 1H), 7.28-7.22 (m, 2H), 5.57 (s, 2H), 2.61 (s, 3H), 2.37 (s, 3H). ^{13}C NMR (101 MHz, $CDCl_3$): δ 162.66, 149.07, 144.08, 138.60, 138.10, 137.70, 132.84, 129.23 × 2, 129.06 × 2, 127.97 × 2, 126.33, 120.95 × 2, 115.92, 111.76, 91.88, 69.33, 21.25, 12.45. HRMS (ESI) *m/z* calcd $C_{22}H_{18}N_4O^+$ $[M + H]^+$: 355.1514, found 355.1549, error 9.9 ppm.

6-(benzyloxy)-3-methyl-1-phenyl-1H-pyrazolo[3,4-b]pyridine-5-carbonitrile (12h). Compound **12h** was prepared in 87% yield from **11** and ethyl cyanoacetate following a similar procedure to that described for synthesis of **12a**. Purity: 98.5%. ^{1}H NMR (500 MHz, DMSO-d_6): δ 8.28 (s, 1H), 8.16-8.13 (m, *J* = 13.9 *Hz*, 3H), 7.52-7.50 (m, *J* = 7.4 *Hz*, 2H), 7.47-7.40 (m, 4H), 7.35-7.32 (m, *J* = 14.7 *Hz*, 1H), 5.55 (s, 2H), 2.51 (s, 3H). HRMS (ESI) *m/z* calcd $C_{21}H_{16}N_4O^+$ $[M + H]^+$: 341.1324, found 341.1349, error 7.3 ppm.

3-Methyl-1-phenyl-6-((4-(trifluoromethyl)benzyl)oxy)-1H-pyrazolo[3,4-b]pyridine-5-carbonitrile (12i). Compound **12i** was prepared in 92% yield from **11** and ethyl cyanoacetate following a similar procedure to that described for synthesis of **12a**. Purity: 97.4%.^{1}H NMR (400 MHz, $CDCl_3$): δ 8.26 (s, 1H), 8.12-8.09 (m, 2H), 7.60-7.52 (m, 2H), 7.48-7.44 (m, 2H), 7.37-7.35 (m, *J* = 7.2 *Hz*, 1H), 7.23-7.20 (m, *J* = 7.9 *Hz*, 2H), 5.64 (s, 2H), 2.61 (s, 3H). ^{13}C NMR (101 MHz, $CDCl_3$): δ 164.26, 148.47, 139.70, 138.45, 137.24, 137.08, 132.54, 129.26 × 2, 128.13 × 2, 127.40 × 2, 126.21, 124.16, 120.33 × 2, 115.78, 113.26, 91.64, 68.55, 12.47. HRMS (ESI) *m/z* calcd $C_{22}H_{15}F_3N_4O^+$ $[M + H]^+$: 409.1232, found 409.1198, error -8.3 ppm.

General Procedure for the Synthesis of 9 and 13a-i.

(Z)-6-((2-fluorobenzyl)oxy)-N'-hydroxy-3-methyl-1-phenyl-1H-pyrazolo[3,4-b]pyridine-5-carboximidamide (13a). To a solution of **12a** (35 g, 98 mmol) in ethyl alcohol (300 mL) were

added hydroxylamine hydrochloride (20.4 g, 294 mmol) and N, N-diisopropylethylamine (51.3 mL, 294 mmol) under argon at room temperature. The mixture was refluxed for 18 h under argon monitoring by TLC. After the residue was cooled to room temperature, and filtered to provide filter cake as the product **13a** (20.4 g). The solvent was removed by vacuum distillation. The solid was purified by silica gel column chromatography (DCM/MeOH, 100:1) to provide **13a** (26.9 g) combined two batches as a white solid. Yield: 77%. Purity: 99%.^{1}H NMR (500 MHz, DMSO-d_6): δ 9.52 (s, 1H), 8.28 (s, 1H), 8.15 (d, J = 7.8 *Hz*, 2H), 7.62 (m, 1H), 7.52 (t, J = 8.0 *Hz*, 2H), 7.42-7.38 (m, 1H), 7.30 (m, 2H), 7.21 (t, J = 7.5 *Hz*, 1H), 5.81 (br s, 2H), 5.62 (s, 2H), 2.55 (s, 3H). ^{13}C NMR (126 MHz, DMSO-d_6): δ 160.67, 160.56, 150.03, 148.16, 144.03, 139.44, 133.49, 130.46, 130.38, 129.60 × 2, 125.78, 124.96, 124.44, 119.90 × 2, 115.76, 113.85, 112.03, 62.56, 12.63. HRMS (ESI) *m/z* calcd $C_{21}H_{18}FN_5O_2^+$ $[M + H]^+$: 392.1445, found 392.1509, error 16.3 ppm.

Compounds **9** and **13b-i** were prepared according to the similar procedure that described for synthesis of **13a**, and these compounds were used directly in the next step without further purification.

General Procedure for the Synthesis of 10 and 14a-i.

6-((2-fluorobenzyl)oxy)-3-methyl-1-phenyl-1H-pyrazolo[3,4-b]pyridine-5-carboximidamide (14a). To a solution of **13a** (28 g, 72 mmol) in acetic acid (300 mL) was added zinc powder portions (30 g, 624 mmol) at room temperature. The mixture was stirred at room temperature for 8 h until the reaction was completely monitoring by TLC. The suspension was filtered and the filtrate was evaporated under vacuum to afford the crude product (35 g), which was poured into 1 N aqueous NaOH (500 mL). The mixture was filtered to provide filter cake (26.8 g), which was purified by silica gel column chromatography (DCM/MeOH, 15:1 to 10:1) to provide **14a** (26.9 g) as a white

solid. Yield: 81%. Purity: 98.5%. ^{1}H NMR (400 MHz, DMSO-d_6): δ 9.29 (br s, 3H), 8.71 (s, 1H), 8.14 (dd, *J* = 8.7, 1.1 *Hz*, 2H), 7.65-7.55 (m, 3H), 7.48-7.40 (m, 1H), 7.37-7.22 (m, 3H), 5.64 (s, 2H), 2.59 (s, 3H). ^{13}C NMR (101 MHz, DMSO-d_6): δ 163.86, 160.65, 159.69, 149.02, 144.93, 138.94, 135.73, 130.85, 130.76, 129.75 × 2, 126.44, 124.99, 123.73, 120.36 × 2, 115.88, 111.67, 108.86, 63.35, 12.70. HRMS (ESI) *m/z* calcd $C_{21}H_{18}FN_5O^+$ [M + H]$^+$: 376.1495, found 376.1567, error 19.1 ppm.

Compounds **10** and **14b-i** were prepared according to the similar procedure that described for synthesis of **14a**, and these compounds were used directly in the next step without further purification.

General Procedure for the Synthesis of 1, 2, 21a-e, 30 and 31a-f.

2-(6-((2-fluorobenzyl)oxy)-3-methyl-1-phenyl-1H-pyrazolo[3,4-b]pyridin-5-yl)pyrimidine-4,6-diamine (21a). To a solution of **14a** (0.6 g, 1.6 mmol) in MeOH (5 mL) and 1,4-dioxane (10 mL) was added malononitrile (0.11 g, 1.6 mmol) at room temperature. The reaction was stirred at 130 °C under microwave radiation for 2 h as monitor by TLC. Then the solvent was evaporated under reduced pressure, the residue was purified by silica gel column chromatography (DCM/MeOH, 30:1) to provide product **21a** (0.36 g) as a white solid. Yield: 81%. Purity: 97%. ^{1}H NMR (500 MHz, DMSO-d_6): δ 8.30 (s, 1H), 8.15 (d, *J* = 7.9 *Hz*, 2H), 7.68 (t, *J* = 7.2 *Hz*, 1H), 7.52 (t, *J* = 7.9 *Hz*, 2H), 7.35 (m, 1H), 7.31-7.25 (m, 2H), 7.19 (t, *J* = 7.4 *Hz*, 1H), 6.17 (br s, 4H), 5.62 (s, 2H), 5.42 (s, 1H), 2.55 (s, 3H). ^{13}C NMR (101 MHz, DMSO-d_6): δ 164.42, 163.52, 160.55, 160.10, 147.88, 144.01, 139.55, 133.43, 129.84, 129.76, 129.65, 129.54 × 2, 125.65, 125.00, 124.98, 121.04, 119.82 × 2, 115.48, 111.88, 81.53, 61.75, 12.67. HRMS (ESI) *m/z* calcd $C_{24}H_{20}FN_7O^+$ [M + H]$^+$: 442.1713, found 442.1769, error 12.7 ppm.

5-(4,6-diaminopyrimidin-2-yl)-3-methyl-1-phenyl-1H-pyrazolo[3,4-b]pyridin-6-ol(1). Compound **1** was prepared in 41% from **14b** and malononitrile following a similar procedure to that described for **21a**. Purity: 98%.^{1}H NMR (500 MHz, DMSO-d_6): δ 9.01 (s, 1H), 8.25 (d, J = 7.7 *Hz*, 2H), 7.57-7.49 (m, 2H), 7.27 (dd, J = 8.0, 4.9 *Hz*, 1H), 6.75 (br s, 4H), 5.44 (s, 1H), 2.56 (s, 3H). ^{13}C NMR (126 MHz, DMSO-d_6): δ 166.18 × 2, 162.47, 161.41, 150.71, 144.52, 139.77, 132.06, 129.46 × 2, 125.48, 120.20 × 2, 111.60, 110.89, 81.05, 12.75. HRMS (ESI) *m/z* calcd $C_{17}H_{15}N_7O^+$ $[M + H]^+$: 334.1338, found 334.1332, error 1.8 ppm.

2-(3-methyl-6-((2-methylbenzyl)oxy)-1-phenyl-1H-pyrazolo[3,4-b]pyridin-5-yl)pyrimidine-4,6-diamine (2). Compound **2** was prepared in 52% from **14e** and malononitrile following a similar procedure to that described for **21a**. Purity: 98%.^{1}H NMR (500 MHz, DMSO-d_6): δ 8.26 (s, 1H), 8.19 (d, J = 8.1 *Hz*, 2H), 7.53 (m, 3H), 7.29 (t, J = 7.4 *Hz*, 1H), 7.18 (m, 3H), 6.12 (br s, 4H), 5.53 (s, 2H), 5.41 (s, 1H), 2.54 (s, 3H), 2.40 (s, 3H). ^{13}C NMR (126 MHz, DMSO-d_6): δ 164.40 × 2, 163.69, 160.95, 148.06, 143.95, 139.65, 136.60, 135.67, 133.12, 130.33, 129.53 × 2, 128.22, 127.98, 126.12, 125.61, 121.22, 119.93 × 2, 111.66, 81.58, 66.58, 19.12, 12.68. HRMS (ESI) *m/z* calcd $C_{25}H_{23}N_7O^+$ $[M + H]^+$: 438.1964, found 438.2040, error 17.3 ppm.

2-(6-((2-fluorobenzyl)oxy)-3-methyl-1-phenyl-1H-pyrazolo[3,4-b]pyridin-5-yl)-5-morpholinopyrimidine-4,6-diamine (21b). Compound **21b** was prepared in 49% from **14a** and **20a** following a similar procedure to that described for **21a**. Purity: 99%.^{1}H NMR (500 MHz, DMSO-d_6): δ 8.31 (s, 1H), 8.11 (d, J = 7.8 *Hz*, 2H), 7.67 (m, 1H), 7.52 (t, J = 7.9 *Hz*, 2H), 7.36-7.31 (m, 1H), 7.28 (dd, J = 16.6, 9.0 *Hz*, 2H), 7.18 (t, J = 7.4 *Hz*, 1H), 6.04 (br s, 4H), 5.62 (s, 2H), 3.83-3.67 (m, 4H), 3.01-2.91 (m, 4H), 2.53 (m, 3H). ^{13}C NMR (126 MHz, DMSO-d_6): δ 161.03, 160.50, 160.05, 159.97, 147.88, 143.98, 139.55, 133.55, 129.81, 129.74, 129.64, 129.52 × 2, 125.65,

125.03, 125.01, 120.69, 119.82 × 2, 115.47, 111.89, 106.81, 67.62 × 2, 61.74, 48.39 × 2, 12.63. HRMS (ESI) *m/z* calcd $C_{28}H_{27}FN_8O_2^+$ $[M + H]^+$: 527.2241, found 527.2285, error 8.3 ppm.

2-(6-((2-fluorobenzyl)oxy)-3-methyl-1-phenyl-1H-pyrazolo[3,4-b]pyridin-5-yl)-5-(piperidin-1-yl)pyrimidine-4,6-diamine (21c). Compound **21c** was prepared in 54% from **14a** and **20b** following a similar procedure to that described for **21a**. Purity: 98%.^{1}H NMR (500 MHz, DMSO-d_6): δ 8.32 (s, 1H), 8.13 (d, *J* = 8.4 *Hz*, 2H), 7.68 (t, *J* = 7.6 *Hz*, 1H), 7.51 (t, *J* = 8.0 *Hz*, 2H), 7.36-7.22 (m, 3H), 7.18 (t, *J* = 7.4 *Hz*, 1H), 5.94 (br s, 4H), 5.63 (s, 2H), 2.93 (m, 4H), 2.54 (s, 3H), 1.65 (m, 4H), 1.53 (m, 2H). ^{13}C NMR (126 MHz, DMSO-d_6): δ 160.87, 160.50, 160.09, 159.67, 147.85, 143.98, 139.55, 133.59, 129.80, 129.73, 129.59 × 2, 129.53, 125.65, 125.04, 125.01, 120.73, 119.80 × 2, 115.48, 111.90, 108.21, 61.74, 49.10 × 2, 27.31 × 2, 23.77, 12.63. HRMS (ESI) *m/z* calcd $C_{29}H_{29}FN_8O^+$ $[M + H]^+$: 525.2448, found 525.2511, error 12.0 ppm.

2-(6-((2-fluorobenzyl)oxy)-3-methyl-1-phenyl-1H-pyrazolo[3,4-b]pyridin-5-yl)-5-(pyrrolidin-1-yl)pyrimidine-4,6-diamine (21d). Compound **21d** was prepared in 46% from **14a** and **20c** following a similar procedure to that described for **21a**. Purity: 97%.^{1}H NMR (500 MHz, DMSO-d_6): δ 8.32 (s, 1H), 8.12 (d, *J* = 7.9 *Hz*, 2H), 7.67 (t, *J* = 7.4 *Hz*, 1H), 7.51 (t, *J* = 7.7 *Hz*, 2H), 7.37-7.25 (m, 3H), 7.18 (t, *J* = 7.3 *Hz*, 1H), 5.95 (br s, 4H), 5.63 (s, 2H), 3.02 (s, 4H), 2.54 (s, 3H), 1.94 (s, 4H). ^{13}C NMR (126 MHz, DMSO-d_6): δ 161.38, 160.44, 160.10, 159.58, 147.84, 143.98, 139.52, 133.56, 129.82, 129.76, 129.65, 129.53 × 2, 125.66, 125.02, 124.99, 120.63, 119.79 × 2, 115.50, 111.90, 103.35, 61.79, 47.58 × 2, 25.69 × 2, 12.63. HRMS (ESI) *m/z* calcd $C_{28}H_{27}FN_8O^+$ $[M + H]^+$: 511.2292, found 511.2339, error 9.2 ppm.

2-(6-((2-fluorobenzyl)oxy)-3-methyl-1-phenyl-1H-pyrazolo[3,4-b]pyridin-5-yl)-N^5,N^5-dimethylpyrimidine-4,5,6-triamine (21e). Compound **21e** was prepared in 44% from **14a** and **20d**

following a similar procedure to that described for **21a**. Purity: 98%.^{1}H NMR (500 MHz, DMSO-d_6): δ 8.31 (s, 1H), 8.13 (d, J = 8.1 *Hz*, 2H), 7.67 (t, J = 7.0 *Hz*, 1H), 7.51 (t, J = 7.7 *Hz*, 2H), 7.33 (dd, J = 10.3, 4.6 *Hz*, 1H), 7.30-7.25 (m, 2H), 7.18(m, 1H t, J = 7.4 *Hz*, 1H), 5.99 (br s, 4H), 5.63 (s, 2H), 2.69 (s, 6H), 2.54 (s, 3H). ^{13}C NMR (126 MHz, DMSO-d_6): δ 160.81, 160.46, 160.08, 159.63, 147.83, 143.97, 139.54, 133.54, 129.79, 129.72, 129.62, 129.52 × 2, 125.63, 125.05, 125.02, 120.75, 119.78 × 2, 115.47, 111.89, 107.87, 61.71, 41.19 × 2, 12.64. HRMS (ESI) *m/z* calcd $C_{26}H_{25}FN_8O^+$ $[M + H]^+$: 485.2135, found 485.2186, error 10.5 ppm.

5-(4,6-diamino-5-morpholinopyrimidin-2-yl)-7-(2-fluorobenzyl)-3-methyl-1-phenyl-1,7-dihydro-6H-pyrazolo[3,4-b]pyridin-6-one (30). Compound **30** was prepared in 41% from **10** and **20a** following a similar procedure to that described for **21a**. Purity: 99%. ^{1}H NMR (400 MHz, DMSO-d_6): δ 8.16 (s, 1H), 7.45-7.40 (m, 1H), 7.30-7.16 (m, 5H), 7.08-6.94 (m, 2H), 6.57 (t, J = 7.3 *Hz*, 1H), 6.10 (br s, 4H), 5.06 (s, 2H), 3.77-3.69 (m, 4H), 2.98-2.88 (m, 4H), 2.39 (s, 3H). ^{13}C NMR (101 MHz, DMSO-d_6): δ 160.69 × 2, 160.50, 159.89, 159.87, 144.96, 142.32, 138.70, 133.38, 130.01, 129.45, 129.04 × 2, 128.21 × 2, 127.04, 124.70, 123.36, 123.10 × 2, 115.45 × 2, 106.63, 105.02, 67.58 × 2, 48.30, 21.65 × 2, 11.73. HRMS (ESI) *m/z* calcd $C_{28}H_{27}FN_8O_2^+$ $[M + H]^+$: 527.2241, found 527.2337, error 18.2 ppm.

2-(6-((3-fluorobenzyl)oxy)-3-methyl-1-phenyl-1H-pyrazolo[3,4-b]pyridin-5-yl)pyrimidine-4,6-diamine (31a). Compound **31a** was prepared in 43% from **14c** and malononitrile following a similar procedure to that described for **21a**. Purity: 99%.^{1}H NMR (400 MHz, DMSO-d_6): δ 8.33 (s, 1H), 8.17 (dd, J = 8.7, 1.0 *Hz*, 2H), 7.57-7.51 (m, 2H), 7.45-7.38 (m, 3H), 7.29 (m, 1H), 7.15-7.08 (m, 1H), 6.21 (br s, 4H), 5.56 (s, 2H), 5.44 (s, 1H), 2.55 (s, 3H). ^{13}C NMR (101 MHz, DMSO-d_6): δ 164.33 × 2, 163.34, 162.47, 160.67, 147.99, 144.03, 141.04, 139.55, 133.45, 130.76, 129.59 × 2,

125.61, 123.14, 120.75, 119.88 × 2, 114.46, 113.99, 111.87, 81.48, 67.21, 12.67. HRMS (ESI) *m/z* calcd $C_{24}H_{20}FN_7O^+$ $[M + H]^+$: 442.1713, found 442.1789, error 17.2 ppm.

2-(6-((4-fluorobenzyl)oxy)-3-methyl-1-phenyl-1H-pyrazolo[3,4-b]pyridin-5-yl)pyrimidine-4,6-diamine (31b). Compound **31b** was prepared in 43% from **14d** and malononitrile following a similar procedure to that described for **21a**. Purity: 98%.^{1}H NMR (500 MHz, DMSO-d_6): δ 8.29 (s, 1H), 8.19 (d, *J* = 7.7 *Hz*, 2H), 7.63 (dd, *J* = 8.6, 5.6 *Hz*, 2H), 7.55 (t, *J* = 8.0 *Hz*, 2H), 7.30 (t, *J* = 7.4 Hz, 1H), 7.23-7.17 (m, 2H), 6.15 (br s, 4H), 5.53 (s, 2H), 5.42 (s, 1H), 2.55 (s, 3H, -CH_3). ^{13}C NMR (126 MHz, DMSO-d_6): δ 164.43 × 2, 163.58, 161.93, 160.86, 148.05, 143.97, 139.61, 134.18, 133.29, 129.58 × 2, 129.57 × 2, 125.59, 121.06, 119.90 × 2, 115.49 × 2, 111.78, 81.55, 67.27, 12.66. HRMS (ESI) *m/z* calcd $C_{24}H_{20}FN_7O^+$ $[M + H]^+$: 442.1713, found 442.1789, error 17.2 ppm.

2-(3-methyl-6-((3-methylbenzyl)oxy)-1-phenyl-1H-pyrazolo[3,4-b]pyridin-5-yl)pyrimidine-4,6-diamine (31c). Compound **31c** was prepared in 54% from **14f** and malononitrile following a similar procedure to that described for **21a**. Purity: 98%.^{1}H NMR (500 MHz, DMSO-d_6): δ 8.27 (s, 1H), 8.21 (d, *J* = 7.8 *Hz*, 2H), 7.54 (t, *J* = 8.0 *Hz*, 2H), 7.39 (s, 1H), 7.35-7.27 (m, 2H), 7.24 (t, *J* = 7.6 *Hz*, 1H), 7.08 (d, *J* = 7.5 *Hz*, 1H), 6.18 (br s, 4H), 5.49 (s, 2H), 5.42 (s, 1H), 2.55 (s, 3H), 2.30 (s, 3H). ^{13}C NMR (126 MHz, DMSO-d_6): δ 164.42 × 2, 163.58, 160.98, 148.09, 143.96, 139.64, 137.81, 137.77, 133.18, 129.58 × 2, 128.60, 128.41, 128.12, 125.56, 124.50, 121.07, 119.90 × 2, 111.70, 81.52, 67.98, 21.51, 12.67. HRMS (ESI) *m/z* calcd $C_{25}H_{23}N_7O^+$ $[M + H]^+$: 438.1964, found 438.2081, error 26.7 ppm.

2-(3-methyl-6-((4-methylbenzyl)oxy)-1-phenyl-1H-pyrazolo[3,4-b]pyridin-5-yl)pyrimidine-4,6-diamine (31d). Compound **31d** was prepared in 52% from **14g** and malononitrile following a similar procedure to that described for **21a**. Purity: 98%.^{1}H NMR (500 MHz, DMSO-d_6): δ 8.26 (s,

1H), 8.20 (d, *J* = 7.7 *Hz*, 2H), 7.54 (t, *J* = 8.0 *Hz*, 2H), 7.43 (d, *J* = 7.9 *Hz*, 2H), 7.29 (t, *J* = 7.4 *Hz*, 1H), 7.17 (d, *J* = 7.9 *Hz*, 2H), 6.15 (br s, 4H), 5.49 (s, 2H), 5.41 (s, 1H), 2.54 (s, 3H), 2.28 (s, 3H). ^{13}C NMR (126 MHz, DMSO-d_6): δ 164.37 × 2, 163.57, 160.99, 148.08, 143.94, 139.63, 136.93, 134.85, 133.14, 129.59 × 2, 129.27 × 2, 127.57 × 2, 125.57, 121.09, 119.89 × 2, 111.66, 81.52, 67.92, 21.20, 12.66. HRMS (ESI) *m/z* calcd $C_{25}H_{23}N_7O^+$ [M + H]$^+$: 438.1964, found 438.2041, error 17.6 ppm.

2-(6-(benzyloxy)-3-methyl-1-phenyl-1H-pyrazolo[3,4-b]pyridin-5-yl)pyrimidine-4,6-diamine (31e). Compound **31e** was prepared in 49% from **14h** and malononitrile following a similar procedure to that described for **21a**. Purity: 97%.^{1}H NMR (500 MHz, DMSO-d_6): δ 8.28 (s, 1H), 8.17 (d, *J* = 8.0 *Hz*, 2H), 7.54 (m, 4H), 7.37 (t, *J* = 7.5 *Hz*, 2H), 7.28 (m, 2H), 6.19 (br s, 4H), 5.54 (s, 2H), 5.42 (s, 1H), 2.55 (s, 3H). ^{13}C NMR (126 MHz, DMSO-d_6): δ 164.34 × 2, 163.49, 160.90, 148.04, 143.97, 139.58, 137.96, 133.24, 129.60 × 2, 128.72 × 2, 127.78, 127.39 × 2, 125.59, 120.99, 119.88 × 2, 111.71, 81.50, 67.96, 12.67. HRMS (ESI) *m/z* calcd $C_{24}H_{21}N_7O^+$ [M + H]$^+$: 424.1808, found 424.1886, error 18.4 ppm.

2-(3-methyl-1-phenyl-6-((4-(trifluoromethyl)benzyl)oxy)-1H-pyrazolo[3,4-b]pyridin-5-yl)pyrimidine-4,6-diamine (31f). Compound **31f** was prepared in 51% from **14i** and malononitrile following a similar procedure to that described for **21a**. Purity: 98%. ^{1}H NMR (500 MHz, DMSO-d_6): δ 8.33 (s, 1H), 8.14 (d, *J* = 7.7 Hz, 2H), 7.87-7.74 (dd, *J* = 40.4, 8.1 *Hz*, 4H), 7.53 (t, *J* = 8.0 *Hz*, 2H), 7.29 (t, *J* = 7.4 *Hz*, 1H), 6.20 (br s, 4H), 5.65 (s, 2H), 5.43 (s, 1H), 2.54 (s, 3H). ^{13}C NMR (126 MHz, DMSO-d_6): δ 164.41 × 2, 163.43, 160.63, 147.95, 144.03, 143.08, 139.53, 133.49, 129.59 × 2, 128.15, 127.79 × 2, 125.88, 125.60 × 2, 123.72, 120.85, 119.84 × 2, 111.93, 81.52, 67.14, 12.65. HRMS (ESI) *m/z* calcd $C_{25}H_{20}F_3N_7O^+$ [M + H]$^+$: 492.1681, found 492.1762, error 16.5 ppm.

2-(6-((2-fluorobenzyl)oxy)-3-methyl-1-phenyl-1H-pyrazolo[3,4-b]pyridin-5-yl)-5-nitrosopyrimidine-4,6-diamine (23). To a solution of **22** (16.3 g, 39 mmol) in methanol (120 mL) was added **16** (8 g, 39 mmol) slowly at room temperature, and white precipitate was formed in the mixture. The reaction was stirred at room temperature for 2 h until the precipitation is completely. The solvent was evaporated under reduced pressure to afford yellow solid (18 g), which was stirred at 130 °C for 30 min in 2-methylpyridine as monitor by TLC. Then the solvent was concentrated in vacuo, the residue was purified by silica gel column chromatography (petroleum ether/EtOAc, 2:1) to provide product **23** (10.3 g) as a deep-green solid. Yield: 55%. Purity: 98%. ^{1}H NMR (500 MHz, $CDCl_3$): δ 10.18 (s, 1H), 9.21 (s, 1H), 8.56 (s, 1H), 8.53 (s, 1H), 8.18 (s, 1H), 8.13 (d, *J* = 7.9 *Hz*, 2H), 7.70 (t, *J* = 6.9 Hz, 1H), 7.54 (t, *J* = 7.9 *Hz*, 2H), 7.31 (m, 3H), 7.20 (t, *J* = 7.5 Hz, 1H), 5.65 (s, 2H), 2.57 (s, 3H). ^{13}C NMR (101 MHz, DMSO-d_6): δ 164.42, 163.52, 160.55, 160.10, 147.88, 144.01, 139.55, 133.43, 129.84, 129.76, 129.65, 129.54 × 2, 125.65, 125.00, 124.98, 121.04, 119.82 × 2, 115.48, 111.88, 81.53, 61.75, 12.67. HRMS (ESI) *m/z* calcd $C_{24}H_{19}FN_8O_2^+$ $[M + H]^+$: 471.1615, found 471.1690, error 15.9 ppm.

2-(6-((2-fluorobenzyl)oxy)-3-methyl-1-phenyl-1H-pyrazolo[3,4-b]pyridin-5-yl)pyrimidine-4,5,6-triamine (24). To a solution of **23** (10 g, 21 mmol) in ethyl acetate (100 mL) and acetic acid (50 mL) was added zinc powder in portions (14 g, 210 mmol) at room temperature. The mixture was stirred at room temperature for 10 h until the reaction was completely monitoring by TLC. The suspension was filtered and the filtrate was evaporated under vacuum to afford the crude product (11.2 g), which was poured into 1 N aqueous NaOH (200 mL). The mixture was filtered and the filtrate was concentrated under reduced pressure, the residue was purified by silica gel column chromatography (DCM/MeOH, 30:1) to provide **24** (6.5 g) as a yellow solid. Yield: 67%. Purity:

98%. ^{1}H NMR (500 MHz, DMSO-d_6): δ 8.25 (s, 1H), 8.16 (d, J = 7.8 *Hz*, 2H), 7.70 (t, J = 7.2 *Hz*, 1H), 7.51 (t, J = 8.0 *Hz*, 2H), 7.36-7.32 (m, 1H), 7.30-7.25 (m, 2H), 7.19 (t, J =7.4 *Hz*, 1H), 5.76 (br s, 4H), 5.61 (s, 2H), 3.97 (br s, 2H), 2.53 (s, 3H). ^{13}C NMR (126 MHz, DMSO-d_6): δ 160.68, 160.10, 152.57, 151.95 × 2, 147.69, 143.84, 139.62, 133.14, 129.80, 129.73, 129.53 × 2, 125.57, 125.05, 125.02, 121.04, 119.75 × 2, 115.45, 111.95, 106.02, 61.71, 12.69. HRMS (ESI) *m/z* calcd $C_{24}H_{21}FN_8O^+$ $[M + H]^+$: 457.1822, found 457.1907, error 18.6 ppm.

General Procedure for the Synthesis of 25a and 27.

N-(4,6-diamino-2-(6-((2-fluorobenzyl)oxy)-3-methyl-1-phenyl-1H-pyrazolo[3,4-b]pyridin-5-yl)pyrimidin-5-yl)acetamide (25a). To a solution of **24** (0.5 g, 1.1 mmol) in CH_3CN (40 mL) was added anhydrous potassium carbonate (0.5 g, 3.6 mmol) at room temperature, then acetyl chloride (0.14 g, 1.7 mmol) was added slowly at 0 °C. The mixture was stirred at 0 °C for 1 h and then stirred at room temperature for 2 h until **24** was consumed completely monitoring by TLC. The suspension was filtered and the filtrate was concentrated under vacuum to afford a crude, which was purified by silica gel column chromatography (DCM/MeOH, 30:1) to provide the product **25a** (0.35 g) as a white solid. Yield: 64%. Purity: 98.6%. ^{1}H NMR (500 MHz, DMSO-d_6): δ 8.61 (s, 1H), 8.33 (s, 1H), 8.15 (d, J = 7.8 *Hz*, 2H), 7.68 (t, J = 7.2 *Hz*, 1H), 7.55-7.47 (t, J = 7.9 *Hz*, 2H), 7.36-7.25 (m, 3H), 7.18 (t, J = 7.4 Hz, 1H), 6.05 (br s, 4H), 5.63 (s, 2H), 2.56 (s, 3H), 2.04 (s, 3H). ^{13}C NMR (126 MHz, DMSO-d_6): δ 169.95, 160.99, 160.49, 160.40, 160.08, 147.88, 143.98, 139.53, 133.41, 129.77, 129.70, 129.63, 129.53 × 2, 125.67, 125.04, 125.02, 120.80, 119.82 × 2, 115.46, 111.87, 94.75, 61.76, 23.64, 12.65. HRMS (ESI) *m/z* calcd $C_{26}H_{23}FN_8O_2^+$ $[M + H]^+$: 499.1928, found 499.2011, error 16.6 ppm.

3-(4,6-diamino-2-(6-((2-fluorobenzyl)oxy)-3-methyl-1-phenyl-1H-pyrazolo[3,4-b]pyridin-5-

yl)pyrimidin-5-yl)oxazolidin-2-one (27). Compound **27** was prepared in 37% from **24** and 2-chloroethyl chloroformate following a similar procedure to that described for **25a**. Purity: 98%.^{1}H NMR (500 MHz, DMSO-d_6): δ 8.33 (s, 1H), 8.13 (d, J =7.8 *Hz*, 2H), 7.66 (t, J = 7.0 *Hz*, 1H), 7.54-7.48 ((t, J=7.9 *Hz*, 2H), 7.36-7.25 (m, 3H, Ar-H), 7.20-7.16 (m, 1H), 6.53 (br s, 4H), 5.65 (s, 2H), 4.47-4.41 (m, 2H), 3.73-3.65 (m, 2H), 2.53 (s, 3H). ^{13}C NMR (101 MHz, DMSO-d_6): δ 162.42, 161.01, 160.09, 160.40, 156.94, 147.90, 144.01, 139.50, 133.54, 129.78, 129.70, 129.59, 129.52 × 2, 125.69, 125.06, 125.04, 120.64, 119.82 × 2, 115.48, 111.79, 93.12, 62.64, 61.77, 43.43, 12.62. HRMS (ESI) *m/z* calcd $C_{27}H_{23}FN_8O_3^+$ [M + H]$^+$: 527.1877, found 527.1960, error 15.7 ppm.

General Procedure for the Synthesis of 25b-d.

Methyl(4,6-diamino-2-(6-((2-fluorobenzyl)oxy)-3-methyl-1-phenyl-1H-pyrazolo[3,4b] pyridin-5-yl)pyrimidin-5-yl)carbamate (25b). To a solution of **24** (1 g, 2.2 mmol) in pyridine (40 mL) was stirred for 1 h at room temperature, then methylclhlorofonmate (0.4 mL, 3.3 mmol) was added slowly at 0 °C. The mixture was stirred at 0 °C for 4 h until the start material **24** was consumed completely as monitor by TLC. The solvent was evaporated *in vacuo* afford a crude which was purified by silica gel column chromatography (DCM/MeOH, 30:1) to provide the product **25b** (0.8 g) as a white solid. Yield: 71%. Purity: 99%. ^{1}H NMR (500 MHz, DMSO-d_6): δ 8.31 (s, 1H), 8.14 (d, J = 7.9 *Hz*, 2H, Ar-H), 7.99 (br s, 1H, -NH-), 7.68 (t, J = 7.3 *Hz*, 1H), 7.51 (t, J = 8.0 *Hz*, 2H), 7.38-7.24 (m, 3H), 7.19 (t, J = 7.4 Hz, 1H), 6.06 (br s, 4H), 5.63 (s, 2H), 3.64 (s, 3H), 2.54 (s, 3H). ^{13}C NMR (126 MHz, DMSO-d_6): δ 161.02, 160.74, 160.48, 160.11, 155.66, 147.90, 143.99, 139.54, 133.41, 129.80, 129.74, 129.70, 129.53 × 2, 125.67, 125.03, 125.00, 120.74, 119.83 × 2, 115.47, 111.86, 94.31, 61.73, 52.22, 12.65. HRMS (ESI) *m/z* calcd $C_{26}H_{23}FN_8O_3^+$ [M + H]$^+$: 515.1877, found 515.1963, error 16.7 ppm.

Butyl(4,6-diamino-2-(6-((2-fluorobenzyl)oxy)-3-methyl-1-phenyl-1H-pyrazolo[3,4-b]pyridin-5-yl)pyrimidin-5-yl)carbamate (25c). Compound **25c** was prepared in 70% from **24** and butyl chloroformate following a similar procedure to that described for **25b**. Purity: 98%. ^{1}H NMR (500 MHz, DMSO-d_6): δ 8.32 (s, 1H), 8.14 (d, J = 7.9 *Hz*, 2H), 7.97 (br s, 1H), 7.68 (t, J = 7.3 *Hz*, 1H), 7.51 (t, J = 7.9 *Hz*, 2H), 7.37-7.25 (m, 3H), 7.18 (t, J = 7.4 *Hz*, 1H), 6.02 (br s, 4H), 5.63 (s, 2H), 4.04 (m, 3H), 2.54 (s, 3H), 1.58 (m, 2H), 1.46-1.36 (m, 2H), 1.27-1.22 (m, 3H). ^{13}C NMR (101 MHz, DMSO-d_6): δ 160.40, 160.26, 160.12, 159.98, 155.33, 148.00, 144.10, 139.47, 133.72, 129.85, 129.76, 129.72, 129.51 × 2, 125.70, 125.03, 125.00, 124.90, 119.82 × 2, 115.48, 111.95, 94.27, 64.64, 61.88, 31.12, 19.14, 14.18, 12.66. HRMS (ESI) *m/z* calcd $C_{29}H_{29}FN_8O_3^+$ $[M + H]^+$: 557.2347, found 557.2439, error 16.5 ppm.

Cyclopentyl(4,6-diamino-2-(6-((2-fluorobenzyl)oxy)-3-methyl-1-phenyl-1H-pyrazolo[3,4b] pyridin-5-yl)pyrimidin-5-yl)carbamate (25d). Compound **25d** was prepared in 52% from **24** and butyl chloroformate following a similar procedure to that described for **25b**. Purity: 99%. ^{1}H NMR (400 MHz, DMSO-d_6): δ 8.31 (s, 1H), 8.13 (d, J = 7.9 *Hz*, 2H), 7.91 (br s, 1H), 7.67 (t, J = 7.3 *Hz*, 1H), 7.51 (t, J = 8.0 *Hz*, 2H), 7.36-7.25 (m, 3H), 7.21-7.16 (m, 1H), 6.01 (br s, 4H), 5.63 (s, 2H), 5.05 (m, 1H), 2.54 (s, 3H), 1.90-1.50 (m, 8H). ^{13}C NMR (126 MHz, DMSO-d_6): δ 160.87, 160.62, 160.47, 160.11, 155.06, 147.89, 143.98, 139.54, 133.42, 129.79, 129.73, 129.68, 129.52 × 2, 125.66, 125.02, 124.99, 120.70, 119.81 × 2, 115.46, 111.86, 94.64, 77.23, 61.77, 32.82 × 2, 23.91 × 2, 12.65. HRMS (ESI) *m/z* calcd $C_{30}H_{29}FN_8O_3^+$ $[M + H]^+$: 569.2347, found 569.2434, error 15.3 ppm.

6-amino-2-(6-((2-fluorobenzyl)oxy)-3-methyl-1-phenyl-1H-pyrazolo[3,4-b]pyridin-5-yl)-7-methyl-7,9-dihydro-8H-purin-8-one (29). To a solution of **25b** (0.55 g, 1.0 mmol) in DMF (40 mL) were added sodium hydride (0.1 g, 4.0 mmol) and methyl iodide (0.1 mL, 1.5 mmol) slowly at

0 °C. Then the mixture was stirred at 0 °C for 2 h and then stirred at room temperature for 2 h until **25b** was consumed completely monitoring by TLC. After the solution was cooled to room temperature, it was poured into a mixture of ice and water (100 mL). The mixture was extracted with ethyl acetate (3 × 100 mL). The combined organic phase was dried over anhydrous sodium sulfate and concentrated, which was purified by silica gel column chromatography (DCM/MeOH, 50:1) to get the product **29** (0.35 g) as a white solid. Yield: 66%. Purity: 99%. ^{1}H NMR (500 MHz, DMSO-d_6): δ 11.62 (s, 1H), 8.37 (s, 1H), 8.16 (d, J = 7.8 *Hz*, 2H), 7.65 (t, J = 7.2 *Hz*, 1H), 7.52 (t, J = 7.9 *Hz*, 2H), 7.38-7.23 (m, 3H), 7.20 (t, J = 7.4 *Hz*, 1H), 6.63 (br s, 2H), 5.63 (s, 2H), 3.49 (s, 3H), 2.54 (s, 3H). ^{13}C NMR (126 MHz, DMSO-d_6): δ 160.53, 160.16, 156.38, 153.53, 148.31, 147.92, 147.65, 144.07, 139.49, 133.98, 129.92, 129.86, 129.75, 129.54 × 2, 125.72, 125.04, 124.86, 119.87 × 2, 115.52, 112.02, 105.26, 61.71, 28.45, 12.68. HRMS (ESI) *m/z* calcd $C_{26}H_{21}FN_8O_2^+$ [M + H]$^+$: 497.1772, found 497.1862, error 18.1 ppm.

Cell Proliferation Assay. HPASMCs (ScienCell, USA) were cultured in D-MEM (High Glucose) supplemented with 20% fetal bovine serum (FBS) and 1% penicillin/streptomycin mixture. HLF1 cells (ScienCell, USA) were cultured in D-MEM/F-12(1:1) supplemented with 10% FBS and 1% penicillin/streptomycin mixture. All cells induced by TGF-β (10 ng/mL, Abbkine) were incubated at 37 °C in a humidified incubator (5% CO_2 in air). Briefly, cells were seeded into 96-well plates at a density appropriate for exponential growth at the start of the assay, and treated with a range of concentrations of compounds for 48 h. Fresh CCK-8 (10 μL, 5 mg/mL, Biosharp) was added to each well and incubated at 37 °C for 4 h. The anti-proliferation activities of **2**, compound C and riociguat against HPASMCs and HLF1 in Figure 4 were induced by hypoxia (1% O_2, 5% CO_2, 94% N_2). The spectrophotometric absorbance of each well was measured by a multi-detection microplate reader

at a wavelength of 490 nm. The IC_{50} was calculated by GraphPad Prism 7 statistical software.

Evaluation on Rat Thoracic Aorta Ring. Male Sprague-Dawley rats (250-280 g) were anesthetized with 10% chloral hydrate (1.25 mL/kg, i.p.) and the thoracic aorta rings were rapidly isolated cleaned of fat and connective tissues, and then cut into rings of 4 mm length. The rings were suspended horizontally between two stainless steel wires and mounted 10 mL organ baths containing 37 °C Krebs-Henseleit solution and constantly gassed with 95% O_2 and 5% CO_2. Each of the rings' end was connected to a force transducer. The aortic rings were stretched with 2 g resting force, equilibrated for 60 min, and then pre-contracted with phenylephrine (10^{-7} M). Each contraction was followed by a series of 10 washing cycles and equilibrated for another 30 min. After the contraction had stabilized, a cumulative concentration-response curve to the candidates (3×10^{-9} - 10^{-6} M, final concentration) was observed. The percentage of relaxed extent to initially contracted extent under 1 μM and the EC_{50} was calculated by GraphPad Prism 7 statistical software.

Cell Migration Assays. HPASMCs and HLF1 cell migration assays were evaluated according to the wound healing test. HPASMCs and HLF1 were cultured in DMEM medium with 20% FBS and 1% penicillin and streptomycin, D-MEM/F-12(1:1) medium with 10% FBS and 1% penicillin and streptomycin, respectively. Cells were seeded in 24-well plate (HPASMCs: 5×10^4 cells; HLF1: 5×10^4 cells) for 24 h and reached almost 100% confluence. Then scratch the cells with a sterile 200 μL pipette tip. Wash the detached cells with PBS and incubate with different medium containing 1% FBS with TGF-β (10 ng/mL, Abbkine) or hypoxia condition (1% O_2, 5% CO_2, 94% N_2) alone or together with **2**, riociguat and compound C, respectively. Migration was allowed to proceed for 24 h at 37 °C in a 5% CO_2 humidified atmosphere. The scratch was auto-photographed with Bio Tek Cytation 5 Cell Imaging Multi-Mode Reader.

HTRF cGMP Assays. For the development of cGMP accumulation assays in HPASMCs, following standard protocols. HTRF cGMP assays were performed according to the manufacturer's instructions (Cisbio, cGMP kits; no. 62GM2PEG). HPASMCs were harvested, resuspended in assay buffer (PBS containing 1 mM IBMX and 0.2% BSA) at a density of 100 000 cells per mL in the absence or presence of 10 μM ODQ, and dispensed into 384-well assay plates (HTRF® no. 66PL384025) at 5 μL per well. Test compounds were solubilized to 100 mM in DMSO as the initial concentration and serially diluted by the diluent of the cGMP kits to achieve a 2 × stock, which was diluted using 10-fold dilutions to generate a 6-point dose-response curve with a top concentration of 200 μM. Diluted compounds were then transferred to a triplicate set of assay plates (5 μL per well). After 1 h incubation at room temperature, 5 μL of cGMP-d2 reagent diluted in lysis buffer was added to each well followed by 5 μL of europium cryptate reagent. Plates were then sealed and incubated at room temperature for 1 h prior to reading on an HTRF® compatible reader (Bio Tek Cytation 5 Cell Imaging Multi-Mode Reader, USA).

PDE-5 Enzymatic Assays[45]. The assays were measured in a buffer including 50 mM Tris-HCl (pH 8.0), 4 mM $MnCl_2$ or 10 mM $MgCl_2$, and 1 mM DTT with ^{3}H-cAMP or ^{3}H-cGMP as the substrate. The reaction worked for 15 min at room temperature and then terminated through adding 0.2 M ZnSO4. The reaction product was precipitated by 0.2 M $Ba(OH)_2$, and the supernatant was the unreacted substrate. The liquid scintillation counter was used to measure the radioactivity of supernatant in 2.5 mL of Ultima Gold liquid scintillation cocktails. The inhibitors were screened at the concentrations of 10 μM, 1 μM, 100 nM. The inhibitory rates were calculated and sildenafil served as the reference compound with an 54.91% inhibition at 2 nM for PDE-5.

HTRF AMPK Assays. AMPK activity was measured following a standard protocol described by

the manufacturer's instructions (Cisbio, KinEASE-STK S1 kit; no. 62ST1PEB). Briefly, human recombinant AMPK (α1β1γ1) protein was pre-phosphorylated by CaMKKβ. The enzyme reaction was performed into 384-well assay plates (HTRF® no. 66PL384025), which contains 0.16 μM STK substrate 1-biotin, 0.8 mmol DTT, 4 mmol $MgCl_2$, 4 μM ATP and corresponding compounds. The reaction was initiated by adding 1 ng/μl p-AMPK (α1β1γ1) protein into the well. Following incubation at 37 ℃ for 1 h, the reaction was terminated by addition of detection reagent contains STK-Antibody labeled with $Eu3^+$-Cryptate and 57.5 nmol/L XL-665, then incubated at room temperature for another 1 h. The fluorescence was measured at 665 nm (XL665) and 620 nm (Eu3+-Cryptate) on an HTRF® compatible reader (Bio Tek Cytation 5 Cell Imaging Multi-Mode Reader, USA), and the ratio was calculated (665/620*10000) for each well and represents the activity of AMPK.

Stability of Compound 2 in the Human and Rat Liver Microsomes[45]. The assays were performed at the Medicilon Company, Shanghai, China. Human and SD rat liver microsomes were purchased from BD Gentest Corporation (Woburn, MA, USA). Compound **2** was dissolved to 10 mM stock solution in 100% DMSO and diluted to a final concentration of 1 μM for the experiments. Ketanserin (Sigma, St. Louis, MO, USA) was used as the positive controls. Liver microsome incubations were conducted in duplicate in 96-well plates. Each well contains 30 μL of 0.1 M potassium phosphate buffer (pH 7.4), 3.0 mM $MgCl_2$, 0.75 mg/mL liver microsomes, and 1.5 μM **2** or the positive control. After 5 min of preincubation at 37 °C, 15 μL of 3 mM NADPH in 0.1 M potassium phosphate buffer was added to initiate the enzymatic reaction. Reactions were terminated at various time points (0, 5, 15, 30, 45 min) by adding 150 μL of ice-cold acetonitrile containing internal standard. A parallel incubation was performed using 0.1 M potassium phosphate buffer (pH

7.4) as the negative control, and reactions were terminated after 45 min incubation. A Shimadzu liquid chromatographic system and an API4000 mass spectrometer equipped with Turbo Ion Spray (ESI) interface (Applied Biosystems, Concord, Ontario, Canada) were used for detection. Analyst 1.5 software packages (Applied Biosystems) were used for control of the LC−MS/MS system, as well as data acquisition and processing.

Pharmacodynamics Effects of Compound 2 against Hypoxia-induced PAH in Animals. Male Sprague-Dawley (SD) rats (weight between 160-200 g) were obtained from Laboratory Animal Center, Xiangya School of Medicine, Central South University (Changsha, China). All experiments were conducted in accordance with the *Guide for the Care and Use of Laboratory Animals*, and the experimental protocol was approved by the Medicine Animal Welfare Committee of Xiangya School of Medicine, Central South University. Rats were acclimated for 7 days, and then were randomly distributed among 4 groups: (i) the control treatment group, (ii) the hypoxia treatment group, (iii) the hypoxia plus riociguat (10 mg/kg) treatment group, and (iv) the hypoxia plus compound **2** (10 mg/kg) treatment group. Rats in the control group were exposed to normobaric normoxia (21% O_2). Rats in the model groups were placed in a chamber and exposed to 10% O_2 continuously for 4 weeks. Compound 2 and riociguat were mixed and suspended in a 0.5% sodium carboxyl methyl cellulose (CMCNa) solution and administrated for 14 days. The rats in the control group and the hypoxia group only received the same dose of CMCNa solution. Sterile food and water were provided in accordance with the institutional guidelines. The rats were fasted overnight and allowed free access to water before each experiment. The right ventricle systolic pressure (RVSP) was measured using right cardiac catheter method. After sacrificing the animals, the right ventricle (RV), left ventricle (LV), and the inter-ventricular septum (S) were dissected from the

heart and were weighed for calculating the ratio of RV/(LV + S) by statistical analysis, which is a key index for evaluating RVH.

Lung Tissue Histological Analysis[31]. Fixed lung tissues with paraffin were sectioned at 5 μm and then stained with conventional hematoxylin-eosin staining (H&E) to measure morphology. A microscopic digital camera and analysis program (Becton Dickinson) was used to capture the images of each group pulmonary arterioles (diameter between 50 and 150 μm). The distance between outer and inner elastic lamina was the definition of PAMT. We calculated the relative PAMT (%) by 100 × 2 PAMT/ External diameter.

Western Blot Analysis. Isolated lung tissues were homogenized and sonicated in RIPA buffer containing with protease and phosphatase inhibitors. The treated tissues were collected and lysed on ice for 30 min, and then which were centrifuged for 15 min at 12 000 rpm under 4 °C. Supernatants were collected for subsequent analysis. The protein concentration was measured with BCA Protein Assay kit (No. BL521A, Biosharp). Equal amounts of protein from each sample (30 μg) were separated by 10% SDS-PAGE and transferred to polyvinylidene fluoride membranes which were blocked with 5% nonfat milk powder for 2 h at room temperature in Tris-buffered saline supplemented with 0.1% Tween 20. Next, the membranes were incubated with mouse anti-α-SMA antibody (1:1000, Abcam, USA) and rabbit anti-β-actin antibody (1:2000, Abbkine, USA) overnight at 4 °C. Then it was incubated with the appropriate secondary antibodies (1:5000, Abbkine, USA) for 2 hours. At last, the bands were detected by western fluorescent detection reagent (No. WBKLS0100, Millipore) and imaged within the ChemiDoc XRS^{+c} imaging system (Bio-Rad).

Molecular Docking. The AMPK-compound C complex (PDB ID: 3aqv) downloaded from the Protein Data Bank was chosen for docking studies. Molecular docking studies were carried out

using MOE 2014 software and performed using the standard default settings with 100 GA runs of molecules. After completion of each docking calculation, the docking poses were analyzed. Surface presentation of the **2** and compound C binding to the active site pocket of AMPK was carried out using the PyMOL surface field. The parameters were used as default and cutoff values of 3.0 Å for hydrogen bonds was set.

Statistics. Values of each variable are expressed as mean ± SEM using GraphPad Prism 7.0, and representative data were selected to generate the figures. Statistical significance was tested using one-way ANOVA with Bonferroni multiple comparisons. Significant difference was assumed at a *P* value of less than 0.05.

ASSOCIATED CONTENT

Supporting Information. The Supporting Information is available free of charge via the Internet at http://pubs.acs.org.

Molecular formula strings and biological data (CSV).

^{1}H NMR, ^{13}C NMR, HRMS and HPLC spectrums of target compounds.

AUTHOR INFORMATION

Corresponding Author

*Phone: +86-731-82650370. Fax: +86-731-82650370. E-mail: qbli@csu.edu.cn.

ORCID

Liqing Hu: 0000-0003-3592-488X

Qi Chang: 0000-0003-0012-3863

Qianbin Li: 0000-0003-4522-3067

Notes

The authors declare no competing financial interest.

ACKNOWLEDGMENTS

This work was supported by the Natural Science Foundation of China (Grants 81573287 and 81773640). We thank the Nuclear Magnetic Resonance Laboratory of Advanced Research Center in Central South University for NMR spectra analysis and Prof. Niansheng Li for kind help in pharmacological experiments. We thank Prof. Hai-Bin Luo from the School of Pharmaceutical Sciences, Sun Yat-Sen University (Guang Zhou) for his help with PDE-5 bioassay.

ABBREVIATIONS USED

ACC, acetyl-CoA carboxylase; AMPK, adenosine monophosphate-activated protein kinase; α-SMA, α-smooth muscle actin; CCK-8, Cell Counting Kit-8; CDDO-Me, bardoxolone methyl; cGMP, cyclic guanosine-3',5'-monophosphate; CMCNa, sodium carboxyl methyl cellulose; DCM, dichloromethane; DMF, dimethylformamide; DMSO dimethylsulfoxide; ET-1, endothelin-1; H&E, hematoxylin and eosin; HLF1, human lung fibroblasts; HTRF, homogeneous time-resolved fluorescence; IBMX, 3-isobutyl-1-methylxanthine; mPAP, mean pulmonary artery pressure; ODQ, 1*H*-[1,2,4]oxadiazolo[4,3-*a*]quinoxalin-1-one; PAH, pulmonary artery hypertension; PAMT, pulmonary artery medial thickness; PASMC, pulmonary arterial smooth muscle cell; PDE-5, phosphodiesterase-5; PKG, protein kinases G; PVR, pulmonary vascular resistance; RVH, right

ventricular hypertrophy; RV/LV+S, right ventricle/left ventricle + septum; RVSP, right ventricular systolic pressure; SAR, structure-activity relationship; sGC, soluble guanylate cyclase; Smad, TGF-β, transforming growth factor; TLC, thin layer chromatography; TMS, tetramethylsilane; VASP, vasodilator-stimulated phosphoprotein.

REFERENCES

(1). Ghofrani, H. A.; Wilkins, M. W.; Rich, S. Uncertainties in the diagnosis and treatment of pulmonary arterial hypertension. *Circulation* **2008,** *118*, 1195-1201.

(2). Boucly, A.; Weatherald, J.; Savale, L.; Jais, X.; Cottin, V.; Prevot, G.; Picard, F.; de Groote, P.; Jevnikar, M.; Bergot, E.; Chaouat, A.; Chabanne, C.; Bourdin, A.; Parent, F.; Montani, D.; Simonneau, G.; Humbert, M.; Sitbon, O. Risk assessment, prognosis and guideline implementation in pulmonary arterial hypertension. *Eur. Respir. J.* **2017,** *50*.

(3). McLaughlin, V. V.; McGoon, M. D. Pulmonary arterial hypertension. *Circulation* **2006,** *114*, 1417-1431.

(4). Lau, E. M. T.; Giannoulatou, E.; Celermajer, D. S.; Humbert, M. Epidemiology and treatment of pulmonary arterial hypertension. *Nat. Rev. Cardiol.* **2017,** *14*, 603-614.

(5). McLaughlin, V. V.; Shah, S. J.; Souza, R.; Humbert, M. Management of pulmonary arterial hypertension. *J. Am. Coll. Cardiol.* **2015,** *65*, 1976-1997.

(6). Badesch, D. B.; McLaughlin, V. V.; Delcroix, M.; Vizza, C. D.; Olschewski, H.; Sitbon, O.; Barst, R. J. Prostanoid therapy for pulmonary arterial hypertension. *J. Am. Coll. Cardiol.* **2004,** *43*, 56S-61S.

(7). Dupuis, J.; Hoeper, M. M. Endothelin receptor antagonists in pulmonary arterial hypertension. *Eur. Respir. J.* **2008,** *31*, 407-415.

(8). Lundberg, J. O.; Gladwin, M. T.; Weitzberg, E. Strategies to increase nitric oxide signalling in cardiovascular disease. *Nat. Rev. Drug Discov.* **2015,** *14*, 623-641.

(9). Raja, S. G.; Raja, S. M. Treating pulmonary arterial hypertension: current treatments and future prospects. *Ther. Adv. Chronic. Dis.* **2011,** *2*, 359-370.

(10). Nakai, T.; Perl, N. R.; Barden, T. C.; Carvalho, A.; Fretzen, A.; Germano, P.; Im, G. Y.; Jin, H.; Kim, C.; Lee, T. W.; Long, K.; Moore, J.; Rohde, J. M.; Sarno, R.; Segal, C.; Solberg, E. O.; Tobin, J.; Zimmer, D. P.; Currie, M. G. Discovery of IWP-051, a novel orally bioavailable sGC stimulator with once-daily dosing potential in humans. *ACS Med. Chem. Lett.* **2016,** *7*, 465-469.

(11). Humbert, M.; Morrell, N. W.; Archer, S. L.; Stenmark, K. R.; MacLean, M. R.; Lang, I. M.; Christman, B. W.; Weir, E. K.; Eickelberg, O.; Voelkel, N. F.; Rabinovitch, M. Cellular and molecular pathobiology of pulmonary arterial hypertension. *J. Am. Coll. Cardiol.* **2004,** *43*, 13S-24S.

(12). Jeffery, T. K.; Wanstall, J. C. Pulmonary vascular remodeling: a target for therapeutic intervention in pulmonary hypertension. *Pharmacol. Ther.* **2001**, *92*, 1-20.

(13). Li, M. X.; Jiang, D. Q.; Wang, Y.; Chen, Q. Z.; Ma, Y. J.; Yu, S. S.; Wang, Y. Signal mechanisms of vascular remodeling in the development of pulmonary arterial hypertension. *J. Cardiovasc. Pharmacol.* **2016,** *67*, 182-190.

(14). Kikuchi, N.; Satoh, K.; Kurosawa, R.; Yaoita, N.; Elias-Al-Mamun, M.; Siddique, M. A. H.; Omura, J.; Satoh, T.; Nogi, M.; Sunamura, S.; Miyata, S.; Saito, Y.; Hoshikawa, Y.; Okada, Y.; Shimokawa, H. Selenoprotein P promotes the development of pulmonary arterial hypertension. *Circulation* **2018,** *138*, 600-623.

(15). Evgenov, O. V.; Pacher, P.; Schmidt, P. M.; Hasko, G.; Schmidt, H. H.; Stasch, J. P. NO-

independent stimulators and activators of soluble guanylate cyclase: discovery and therapeutic potential. *Nat. Rev. Drug Discov.* **2006,** *5*, 755-768.

(16). Choi, S.; Park, M.; Kim, J.; Park, W.; Kim, S.; Lee, D. K.; Hwang, J. Y.; Choe, J.; Won, M. H.; Ryoo, S.; Ha, K.S.; Kwon, Y. G.; Kim, Y, M. TNF-α elicits phenotypic and functional alterations of vascular smooth muscle cells by miR-155-5p-dependent down-regulation of cGMP-dependent kinase 1. *J. Biol. Chem.* **2018**, *293*, 14812-14822.

(17). Sandner, P.; Zimmer, D. P.; Milne, G. T.; Follmann, M.; Hobbs, A.; Stasch, J. P. Soluble Guanylate Cyclase Stimulators and Activators. *Handb Exp Pharmacol*, Springer: New York, **2019**; pp 1-40.

(18). Ghofrani, H. A.; Galie, N.; Grimminger, F.; Grunig, E.; Humbert, M.; Jing, Z. C.; Keogh, A. M.; Langleben, D.; Kilama, M. O.; Fritsch, A.; Neuser, D.; Rubin, L. J.; Group, P. S. Riociguat for the treatment of pulmonary arterial hypertension. *N. Engl. J. Med.* **2013,** *369*, 330-340.

(19). Guha, M. First-in-class guanylate cyclase stimulator approved for PAH. *Nat. Biotechnol.* **2013,** *31*, 1064.

(20). Makowski, C. T.; Rissmiller, R. W.; Bullington, W. M. Riociguat: a novel new drug for treatment of pulmonary hypertension. *Pharmacotherapy* **2015,** *35*, 502-519.

(21). Burks, M.; Stickel, S.; Galie, N. Pulmonary arterial hypertension: combination therapy in practice. *Am. J. Cardiovasc. Drugs* **2018,** *18*, 249-257.

(22). Hardie, D. G.; Ross, F. A.; Hawley, S. A. AMPK: a nutrient and energy sensor that maintains energy homeostasis. *Nat. Rev. Mol. Cell Biol.* **2012,** *13*, 251-262.

(23). Ríos, M.; Foretz, M.; Viollet, B.; Prieto, A.; Fraga, M.; Costoya, J. A.; Señarís, R. AMPK activation by oncogenesis is required to maintain cancer cell proliferation in astrocytic tumors.

Cancer Res. **2013**, 73, 2628-2638.

(24). Ibe, J. C.; Zhou, Q.; Chen, T.; Tang, H.; Yuan, J. X.; Raj, J. U.; Zhou, G. Adenosine monophosphate-activated protein kinase is required for pulmonary artery smooth muscle cell survival and the development of hypoxic pulmonary hypertension. *Am. J. Respir. Cell Mol. Biol.* **2013,** *49*, 609-618.

(25). Zheng, X.; Zheng, W.; Xiong, B.; Huang, J. The efficacy and safety of soluble guanylate cyclase stimulators in patients with heart failure: a systematic review and meta-analysis. *Medicine (Baltimore)* **2018,** *97*, e12709.

(26). Dai, J.; Zhou, Q.; Chen, J.; Rexius-Hall, M. L.; Rehman, J.; Zhou, G. Alpha-enolase regulates the malignant phenotype of pulmonary artery smooth muscle cells via the AMPK-Akt pathway. *Nat. Commun.* **2018,** *9*, 3850.

(27). Shimoda, L. A.; Laurie, S. S. Vascular remodeling in pulmonary hypertension. *J. Mol. Med. (Berl).* **2013,** *91*, 297-309.

(28). Liu, J.; Wang, W.; Wang, L.; Chen, S.; Tian, B.; Huang, K.; Corrigan, C. J.; Ying, S.; Wang, W.; Wang, C. IL-33 initiates vascular remodelling in hypoxic pulmonary hypertension by up-regulating HIF-1alpha and VEGF expression in vascular endothelial cells. *EBioMedicine* **2018,** *33*, 196-210.

(29). Shi, W.; Zhai, C.; Feng, W.; Wang, J.; Zhu, Y.; Li, S.; Wang, Q.; Zhang, Q.; Yan, X.; Chai, L.; Liu, P.; Chen, Y.; Li, M. Resveratrol inhibits monocrotaline-induced pulmonary arterial remodeling by suppression of SphK1-mediated NF-kappaB activation. *Life Sci.* **2018,** *210*, 140-149.

(30). Humbert, M.; Ghofrani, H. A. The molecular targets of approved treatments for pulmonary arterial hypertension. *Thorax* **2016,** *71*, 73-83.

(31). Cheng, Y.; Gong, Y.; Qian, S.; Mou, Y.; Li, H.; Chen, X.; Kong, H.; Xie, W.; Wang, H.; Zhang, Y.; Huang, Z. Identification of a novel hybridization from isosorbide 5-mononitrate and bardoxolone methyl with dual activities of pulmonary vasodilation and vascular remodeling inhibition on pulmonary arterial hypertension rats. *J. Med. Chem.* **2018,** *61*, 1474-1482.

(32). Lourenco, A. L.; Salvador, R. R. S.; Silva, L. A.; Saito, M. S.; Mello, J. F. R.; Cabral, L. M.; Rodrigues, C. R.; Vera, M. A. F.; Muri, E. M. F.; de Souza, A. M. T.; Craik, C. S.; Dias, L. R. S.; Castro, H. C.; Sathler, P. C. Synthesis and mechanistic evaluation of novel N'-benzylidene-carbohydrazide-1H-pyrazolo[3,4-b]pyridine derivatives as non-anionic antiplatelet agents. *Eur. J. Med. Chem.* **2017,** *135*, 213-229.

(33). Follmann, M.; Griebenow, N.; Hahn, M. G.; Hartung, I.; Mais, F. J.; Mittendorf, J.; Schafer, M.; Schirok, H.; Stasch, J. P.; Stoll, F.; Straub, A. The chemistry and biology of soluble guanylate cyclase stimulators and activators. *Angew. Chem. Int. Ed. Engl.* **2013,** *52*, 9442-9462.

(34). Handa, N.; Takagi, T.; Saijo, S.; Kishishita, S.; Takaya, D.; Toyama, M.; Terada, T.; Shirouzu, M.; Suzuki, A.; Lee, S.; Yamauchi, T.; Okada-Iwabu, M.; Iwabu, M.; Kadowaki, T.; Minokoshi, Y.; Yokoyama, S. Structural basis for compound C inhibition of the human AMP-activated protein kinase alpha2 subunit kinase domain. *Acta. Crystallogr. D. Biol. Crystallogr.* **2011,** *67*, 480-487.

(35). Laborde, E.; Macsata, R. W.; Meng, F.; Peterson, B. T.; Robinson, L.; Schow, S. R.; Simon, R. J.; Xu, H.; Baba, K.; Inagaki, H.; Ishiwata, Y.; Jomori, T.; Matsumoto, Y.; Miyachi, A.; Nakamura, T.; Okamoto, M.; Handel, T. M.; Bernard, C. C. Discovery, optimization, and pharmacological characterization of novel heteroaroylphenylureas antagonists of C-C chemokine ligand 2 function. *J. Med. Chem.* **2011,** *54*, 1667-1681.

(36). Voros, A.; Mucsi, Z.; Baan, Z.; Timari, G.; Hermecz, I.; Mizsey, P.; Finta, Z. An experimental

and theoretical study of reaction mechanisms between nitriles and hydroxylamine. *Org. Biomol. Chem.* **2014,** *12*, 8036-8047.

(37). Flesch, D.; Gabler, M.; Lill, A.; Gomez, R. C.; Steri, R.; Schneider, G.; Stark, H.; Schubert-Zsilavecz, M.; Merk, D. Fragmentation of GW4064 led to a highly potent partial farnesoid X receptor agonist with improved drug-like properties. *Bioorg. Med. Chem.* **2015,** *23*, 3490-3498.

(38). Zhang, L. B.; Wang, D. X.; Zhao, L.; Wang, M. X. Synthesis and application of enantioenriched functionalized alpha-tetrasubstituted alpha-amino acids from biocatalytic desymmetrization of prochiral alpha-aminomalonamides. *J. Org. Chem.* **2012,** *77*, 5584-5591.

(39). Boyd, J. P.; Irran, E.; Grohmann, A. Tetrapodal amidoxime ligands I coordination isomerism due to self-complementary dimerization of a pyramidal cobalt(III) coordination module. *Dalton Trans.* **2012,** *41*, 2477-2485.

(40). Wilson, N. S.; Osuma, A. T.; Camp, J. A. V.; Xu, X. A scalable approach to diaminopyrazoles using flow chemistry. *Tetrahedron Letters* **2012,** *53*, 4498-4501.

(41). Jungmann, O.; Pfleiderer, W. Nucleosides part LXVII: synthesis of 4-amino-7(8H)pteridinone-N8-nucleosides-structural analogs of adenosine. *Nucleosides Nucleotides Nucleic Acids* **2009,** *28*, 550-585.

(42). Kikuchi, N.; Satoh, K.; Saito, Y.; Shimokawa, H. Selenoprotein P promotes the development of pulmonary arterial hypertension: a possible novel therapeutic target. *Circulation* **2019**, *139*, 724-725

(43). Sakao, S.; Tatsumi, K. Vascular remodeling in pulmonary arterial hypertension: multiple cancer-like pathways and possible treatment modalities. *Int. J. Cardiol.* **2011,** *147*, 4-12.

(44). Roberto B. Evora, P.; M. Evora, P.; C. Celotto, A.; J. Rodrigues, A.; E. Joviliano, E.

Cardiovascular therapeutics targets on the NO-sGC-cGMP signaling pathway: a critical overview. *Current Drug Targets* **2012**, *13*, 1207-1214.

(45). Wu, D.; Zhang, T.; Chen, Y.; Huang, Y.; Geng, H.; Yu, Y.; Zhang, C.; Lai, Z.; Wu, Y.; Guo, X.; Chen, J.; Luo, H. B. Discovery and optimization of chromeno[2,3-c]pyrrol-9(2H)-ones as novel selective and orally bioavailable phosphodiesterase 5 inhibitors for the treatment of pulmonary arterial hypertension. *J. Med. Chem.* **2017**, *60*, 6622-6637.

(46). Sartore, S.; Chiavegato, A.; Faggin, E.; Franch, R.; Puato, M.; Ausoni, S.; Pauletto, P. Contribution of adventitial fibroblasts to neointima formation and vascular remodeling. *Circulation Research* **2001**, *89*, 1111-1121.

(47). Labrousse-Arias, D.; Castillo-Gonzalez, R.; Rogers, N. M.; Torres-Capelli, M.; Barreira, B.; Aragones, J.; Cogolludo, A.; Isenberg, J. S.; Calzada, M. J. HIF-2alpha-mediated induction of pulmonary thrombospondin-1 contributes to hypoxia-driven vascular remodelling and vasoconstriction. *Cardiovasc. Res.* **2016**, *109*, 115-130.

(48). Xue, J.; Nelin, L. D.; Chen, B. Hypoxia induces arginase II expression and increases viable human pulmonary artery smooth muscle cell numbers via AMPKalpha1 signaling. *Am. J. Physiol. Lung Cell Mol. Physiol.* **2017**, *312*, L568-L578.

(49). Li, X. W.; Du, J.; Hu, G. Y.; Hu, C. P.; Li, D.; Li, Y. J.; Li, X. H. Fluorofenidone attenuates vascular remodeling in hypoxia-induced pulmonary hypertension of rats. *Can. J. Physiol. Pharmacol.* **2014**, *92*, 58-69.

(50). Lang, M.; Kojonazarov, B.; Tian, X.; Kalymbetov, A.; Weissmann, N.; Grimminger, F.; Kretschmer, A.; Stasch, J. P.; Seeger, W.; Ghofrani, H. A.; Schermuly, R. T. The soluble guanylate cyclase stimulator riociguat ameliorates pulmonary hypertension induced by hypoxia and SU5416

in rats. *PLoS One* **2012**, *7*, e43433.

(51). Zheng, H.; Wu, Y.; Sun, B.; Cheng, C.; Qiao, Y.; Jiang, Y.; Zhao, S.; Xie, Z.; Tan, J.; Lou, H. Discovery of furyl/thienyl beta-carboline derivatives as potent and selective PDE5 inhibitors with excellent vasorelaxant effect. *Eur. J. Med. Chem.* **2018**, *158*, 767-780.

(52). Aschner, Y.; Downey, G. P. Transforming growth factor-β: master regulator of the respiratory system in health and disease. *Am. J. Respir. Cell Mol. Biol.* **2016**, *54*, 647-655.

(53). Grasemann, H.; Dhaliwal, R.; Ivanovska, J.; Kantores, C.; McNamara, P. J.; Scott, J. A.; Belik, J.; Jankov, R. P. Arginase inhibition prevents bleomycin-induced pulmonary hypertension, vascular remodeling, and collagen deposition in neonatal rat lungs. *Am. J. Physiol. Lung Cell Mol. Physiol.* **2015**, *308*, L503- L510.

(54). Ranchoux, B.; Antigny, F.; Rucker-Martin, C.; Hautefort, A.; Pechoux, C.; Bogaard, H. J.; Dorfmuller, P.; Remy, S.; Lecerf, F.; Plante, S.; Chat, S.; Fadel, E.; Houssaini, A.; Anegon, I.; Adnot, S.; Simonneau, G.; Humbert, M.; Cohen-Kaminsky, S.; Perros, F. Endothelial-to-mesenchymal transition in pulmonary hypertension. *Circulation* **2015**, *131*, 1006-1018.

(55). Wegener, J. W.; Nawrath, H.; Wolfsgruber, W.; Kühbandner, S.; Werner, C.; Hofmann. F.; Feil, R. cGMP-dependent protein kinase I mediates the negative inotropic effect of cGMP in the murine myocardium. *Circ. Res.* **2002**, *90*, 18-20.

(56). Matei, A. E.; Beyer, C.; Gyorfi, A. H.; Soare, A.; Chen, C. W.; Dees, C.; Bergmann, C.; Ramming, A.; Friebe, A.; Hofmann, F.; Distler, O.; Schett, G.; Distler, J. H. W. Protein kinases G are essential downstream mediators of the antifibrotic effects of sGC stimulators. *Ann. Rheum. Dis.* **2018**, *77*, 459.

(57). Chettimada, S.; Rawat, D. K.; Dey, N.; Kobelja, R.; Simms, Z.; Wolin, M. S.; Lincoln, T. M.;

Gupte, S. A. Glc-6-PD and PKG contribute to hypoxia-induced decrease in smooth muscle cell contractile phenotype proteins in pulmonary artery. *Am. J. Physiol. Lung Cell Mol. Physiol.* **2012**, *303*, L64-L74.`

Table of Contents Graphic